14

Modelling of sand deposition in archaeologically significant reaches of the Colorado River in Grand Canyon, USA

S. Wiele and M. Torizzo

14.1 Introduction

The construction and application of computational models provide a rigorous framework for the study of river mechanics as well as for quantitative predictions that can serve as the basis for informed management decisions regarding environmental issues. Computational models of fluvial processes are typically tailored for particular applications. A balance between data availability, computational efficiency and sufficient accuracy to meet application ends is typically required, especially for models intended to predict the evolution of some fluvial process over time. In modelling the Colorado River in the Grand Canyon, this balance must account for data limitations resulting from the remoteness of the study sites and the computational demands stemming from the multi-dimensional modelling of flow fields with recirculation zones, suspended sand transport and time stepping of changes in sand deposits. The purpose of the Grand Canyon model is to predict deposition rates, volumes and location over a range of discharges and sand supplies to anticipate the consequences of the operation of Glen Canyon Dam and tributary events.

Computational Fluid Dynamics: Applications in Environmental Hydraulics
Edited by P.D. Bates, S.N. Lane and R.I. Ferguson © 2005 John Wiley & Sons, Ltd

The Colorado River corridor in Grand Canyon National Park has been severely altered from its free-flowing state by the construction and closure of Glen Canyon Dam. The once turbid, sediment-laden flow is now clear except during tributary flows. The current average annual sand volume in transport below the first major sediment-contributing tributary below the dam, the Paria River, is about 1.5 million metric tons, or about 6% of the pre-dam sediment load (Topping *et al.*, 2000a). Pre-dam average annual flood peaks of 2420 m^3/s have been typically reduced to the powerplant capacity of 930 m^3/s except on several occasions during exceptional hydrologic conditions or, as of this writing, a single experimental release (see Webb *et al.*, 1999). Winter base flows have been increased from less than about 80 m^3/s prior to the dam construction to about 140 m^3/s under current dam operations. These changes to the flow and sediment characteristics of the river have had direct impacts on dependent resources, such as the preservation of archaeological artefacts, riparian vegetation and endangered species such as the humpback chub and the Kanab Amber snail. The retention of the main-stem sand supply behind Glen Canyon Dam also has led to the erosion of downstream sand deposits that form the substrate for riparian flora and fauna, are used as campsites by riverside visitors to the national park and are an important aesthetic attribute of the natural, formerly unregulated river in the park.

The only tool currently under consideration for mitigating the effects of Glen Canyon Dam on the downstream river corridor is the dam itself. An Environmental Impact Study (EIS; US Department of Interior, 1995) proposed releasing water at discharges in excess of powerplant capacity to entrain and suspend sediment stored at lower elevations within the channel for redeposition at higher elevations along the channel sides. An experimental release from Glen Canyon Dam in 1996 demonstrated that the dam can be operated to restore deposits along the channel sides if sufficient sand is available. The experimental release consisted of a steady discharge of 225 m^3/s for 4 days rising to a steady 1270 m^3/s for 7 days, followed by another steady 225 m^3/s for about 3 1/2 days. As summarized by Schmidt (1999), many of the objectives for a high release contained in an EIS (US Department of Interior, 1995) were achieved by the 1996 release. River guides reported improved camping conditions after the 1996 test flow (Thompson *et al.*, 1997). Kearsley *et al.* (1999) reported an increase in usable campsites from 218 to 299. Studies of aerial photos (Schmidt *et al.*, 1999) and bathymetric measurements before, during and after the test flow (Andrews *et al.*, 1999) documented significant deposition at many sites, along with considerable spatial and temporal variability. Although many sandbars were replenished, sandbars closest to the dam, and therefore with the smallest available sand supply, were more likely to erode (Schmidt, 1999). More recent studies, moreover, have concluded that the channel sand-storage capacity is much less than was posited in the EIS (Topping *et al.*, 2000b) and have suggested that the timing of high flows should be adjusted to follow shortly after tributary inputs (Lucchitta and Leopold, 1999; Rubin *et al.*, 2002) to maximize the use of the available sediment.

Studies of the geomorphology of near-river environments where archaeological sites are located (Hereford *et al.*, 1991, 1993) have concluded that the lower peak discharges and lower sand concentrations since the closure of Glen Canyon Dam have directly or indirectly damaged some of those sites. Hereford *et al.* (1991, 1993) concluded that the high discharges released from the dam during 1983 directly

eroded archaeological sites. They also describe a more pervasive process related to the lowering of base level for side channels. One type of stream channel they describe, their Type 1, consists of short (300–400-m long), steep, ephemeral streams that drain small near main-stem catchments during rainstorms. They concluded that the erosion of sand deposits at the base of these streams since dam closure has lowered the base level of the streams and led to the upstream migration of nick-points. As side streams have deepened and widened, they have encroached upon archaeological sites, and in some cases, the erosion has exposed and damaged the sites. Hereford *et al.* (1991, 1993) proposed that the periodic restoration of sand deposits near river level would raise the base level for these side channels, promoting refilling of the channels that would in turn help preserve the archaeological sites. Thompson and Potochnik (2000), in their extensive study of reaches with abundant artefacts and active gullies, concluded that renewed sand deposition could help preserve some, but not all, sites. Observations soon after the 1996 test flow showed that under the conditions at that time, the terraces containing resources gained sand in some cases, and no harm to these sensitive terrace deposits was reported (Yeatts, 1996).

Hereford *et al.* (1991, 1993) focused on water transport of sediment in gullies in their suggestion that erosion of sand bars near the main-stem shorelines is linked to erosion of archaeological sites. Evidence of local reworking of sand by wind, however, has been documented by several workers and suggests an alternative link between the erosion of sand bar deposits along the channel sides and the formation of artefact-damaging gullies. Aeolian deposits are widespread in many areas within Grand Canyon (Schmidt and Graf, 1990; Hereford *et al.*, 1991, 1993, 1998; Schmidt and Leschin, 1995; Hereford, 1996). Thompson and Potochnik (2000) found that half of the 199 catchments they studied in Marble Canyon, Furnace Flats, the Aisles and Western Grand Canyon had some kind of aeolian deposition, and 42% had active aeolian deposition. The possible significance of aeolian processes in the erosion of streamside sand deposits has been noted in studies of the deposition and longevity of streamside deposits (Howard and Dolan, 1981; Beus *et al.*, 1985; Hereford *et al.*, 1993, 1996; US Department of Interior, 1995; Yeatts, 1998; Schmidt, 1999). Thompson and Potochnik (2000) suggested that wind may be a major mechanism in restoring sand to gullies owing to the evidence of aeolian deposition at many of their sites. They further suggested that aeolian reworking of newly deposited sand onto higher terraces would be significant as long as the supply of sand deposited by the river is available and is not cut off from upper slopes by vegetation. Powell (1897), although concerned more about survival than sediment transport on his pioneering journeys in Grand Canyon, noted in his diaries that fierce flames erupted from campfires as a result of high winds near river level. An implication of the observations of these studies is that streamside sand deposits are an important source for windblown sand. Although some of this windblown sand would be immediately lost to the river, some would be redistributed over the nearby slopes.

The effects of windblown sand would have been made more significant in the pre-dam era as a result of the lower winter river stages, which would expose larger subaerial portions of deposits, coincide with high winter winds and follow the prime season for tributary contributions of bar-forming sand (Cluer, 1995; David J. Topping, US Geological Survey, oral communication, 1999). The infrequent, local, intense rainstorms associated with the initiation and development of gullying

(Hereford *et al.*, 1991, 1993; Thompson and Potochnik, 2000) may have been offset in the pre-dam era by the infilling and healing of incipient gullies by windblown sand.

The mechanism linking channel-side sand deposits with the erosion of upslope artefacts is uncertain and likely to be the subject of ongoing investigation. Nevertheless, the mechanisms described above provide motivation for evaluating the volume and locations of sand deposition in response to sand supplies and dam releases beyond the simple sand-storage concerns that have dominated past sand studies in Grand Canyon. Short of experimenting with a variety of high flows, which is not feasible and would in any case run the risk of permanently damaging cultural resources, the best option is the application of a model that has been demonstrated to represent well the complex flow, sand transport, and erosion and deposition patterns in previous studies.

14.2 Flow and sediment transport model

14.2.1 Model

The numerical methods used in the model are described by Wiele *et al.* (1996) and are based on Patankar's finite volume method (1980), which features a staggered grid and upwind differencing to solve the three equations of motion for the vertically averaged, 2D flow field. A key attribute of the finite volume method is that it conserves mass, a crucial requirement for sediment transport applications. The flow algorithms must contend with complex flow fields, typically including recirculation zones, which generate strong velocity gradients. A diffusion–advection equation is used to calculate the 3D sand concentration field from which the local suspended sand transport can be determined. A turbulence closure is applied to recover the vertical structure of the turbulent mixing and the velocity profile. Local bedload also is calculated on the basis of local shear stress at the bed, critical shear stress and local bed slope. The change in bed configuration over a small time step is calculated from the divergence of the total sand transport rate.

The flow field is calculated by numerically solving the momentum equations in the downstream direction,

$$\frac{\partial u}{\partial t} + u\frac{\partial u}{\partial x} + v\frac{\partial u}{\partial y} - \frac{\partial}{\partial x}\varepsilon\frac{\partial u}{\partial x} - \frac{\partial}{\partial y}\varepsilon\frac{\partial u}{\partial x} + g\left(\frac{\partial h+\eta}{\partial x} - S\right) + \frac{\tau_x}{\rho h} = 0 \tag{14.1}$$

and cross-stream direction,

$$\frac{\partial v}{\partial t} + v\frac{\partial v}{\partial y} + u\frac{\partial v}{\partial x} - \frac{\partial}{\partial y}\varepsilon\frac{\partial v}{\partial y} - \frac{\partial}{\partial x}\varepsilon\frac{\partial u}{\partial x} + g\frac{\partial h+\eta}{\partial y} + \frac{\tau_y}{\rho h} = 0 \tag{14.2}$$

and with the continuity equation

$$\frac{\partial h}{\partial t} + \frac{\partial uh}{\partial x} + \frac{\partial vh}{\partial y} = 0 \tag{14.3}$$

where x is the direction normal to the upstream boundary, y is the direction normal to x, u is the vertically averaged velocity in the x-direction, v is the vertically averaged velocity in the y-direction, h is the flow depth, η is the bed surface elevation, S is the average reach slope, ε is the eddy viscosity, g is gravity, ρ is density of water, and τ_x and τ_y are the shear stresses in the x- and y-directions, respectively. Equations (14.1)–(14.3) are in Cartesian coordinates. For applications to reaches with significant curvature, the equations were modified with the metric of Smith and McLean (1984) for calculations based on an orthogonal curvilinear coordinate system with a variable radius of curvature.

A friction coefficient, c_f, is used to relate the resolved shear stress, τ, to the resolved velocity,

$$\tau = \rho c_f |U| U \tag{14.4}$$

where $U = (u^2 + v^2)^{1/2}$ is the magnitude of the resolved velocity. The x and y components are determined from the relations:

$$\tau_x = \rho c_f u U \tag{14.5}$$

and

$$\tau_y = \rho c_f v U \tag{14.6}$$

The friction coefficient is defined by

$$c_f = \left(\frac{\kappa}{\ln \frac{h}{z_0} - 1} \right)^2 \tag{14.7}$$

where κ is von Karman's constant and z_0 is the roughness parameter. Equation (14.7) is derived by vertically averaging the logarithmic velocity profile (Keulegan, 1938). The value of z_0 at each node depends in part on the thickness of the sand cover. A value for z_0 was initially computed based on bathymetric measurements with $z_0 = 0.1 b_{84}$, where b_{84} is the 84th percentile of the deviations of the local bathymetric measurement from a straight line drawn between two adjacent nodes. The coefficient 0.1 is typically used to relate z_0 to a distribution of gravel sizes. Where the local sand thickness exceeds the z_0 computed from bathymetric records, then the local z_0 was computed based on estimated bedform dimensions, as will be discussed in more detail later.

The eddy viscosity, ε, is defined by

$$\varepsilon(z) = u_* \kappa z (1 - z/h) \tag{14.8}$$

where u_* is the shear velocity $(\tau/\rho)^{1/2}$, and z is the distance above the bed. Equation (14.8) is vertically averaged for use in equations (14.1) and (14.2):

$$\varepsilon = \frac{u_* \kappa h}{6} \tag{14.9}$$

Total load sediment transport equations were found to be far too sensitive to the flow field and yielded physically unreasonable results. Instead, a 3D suspended sand field is calculated using a near-bed boundary condition that is a function of local boundary shear stress. This combination is computationally robust and yields predictions that agree well with measurements. The transport of suspended sand is governed by an advection–diffusion equation:

$$\frac{\partial c}{\partial t} + \frac{\partial cu}{\partial x} + \frac{\partial cv}{\partial y} + \frac{\partial cw}{\partial z} - \frac{\partial}{\partial x}\varepsilon\frac{\partial c}{\partial x} - \frac{\partial}{\partial y}\varepsilon\frac{\partial c}{\partial y} - \frac{\partial}{\partial z}\varepsilon\frac{\partial c}{\partial z} + w_s\frac{\partial c}{\partial z} = 0 \tag{14.10}$$

where c is sand concentration and w_s is sediment settling velocity. The sediment eddy viscosity, ε, in equation (14.10) is assumed to be equal to the momentum eddy viscosity represented by equation (14.8). As with equations (14.1)–(14.3), equation (14.10) was modified for applications to the Lower Tanner and Upper Unkar reaches, which have significant curvature, for application to an orthogonal curvilinear coordinate system using the metric of Smith and McLean (1984).

Equation (14.10) is solved for a given flow field with 11 points in the vertical that are concentrated near the water surface and near the bed to resolve the gradients near the boundaries. The sand transport is represented by the median grain size, d_{50}. The eddy viscosity as a function of z is calculated with equation (14.8). The velocity as a function of z is computed from the logarithmic velocity profile (Keulegan, 1938) from which equation (14.7) is derived. The numerical method used to solve equation (14.10) is similar to the one used for the flow equations (Patankar, 1980) extended to three dimensions.

The lower sediment-concentration boundary condition used in the solution of equation (14.10) is calculated by first determining a reference concentration, c_a, at the top of the bedload layer, where $z = z_a$. The reference concentration, c_a, is determined from the relations of Smith and McLean (1977):

$$c_a = \frac{c_b \gamma s}{1 + \gamma s} \tag{14.11}$$

where c_b is the bed concentration and s is the normalized excess shear stress:

$$s = \frac{\tau_{sf} - \tau_c}{\tau_c} \tag{14.12}$$

where the subscript sf indicates skin friction shear stress and τ_c is critical shear stress for the initiation of significant particle motion (Shields, 1936). The value of the constant γ has been updated to 0.004 by Wiberg (reported by McLean, 1992). The distance above the bed corresponding to c_a, namely z_a, is determined from the expression presented by Dietrich (1982) with coefficients a_1 and a_2 as updated by Wiberg and Rubin (1985)

$$z_a = d\frac{a_1 + T_*}{1 + a_2 T_*} \tag{14.13}$$

where d is grain diameter, T_* is the ratio of the skin friction shear stress to the critical shear stress (τ_{sf}/τ_c), and a_1 is a constant ($a_1 = 0.68$).

The coefficient a_2 is a function of the grain size in centimetres:

$$a_2 = 0.02035(\ln(d))^2 + 0.02203\ln(d) + 0.07090 \tag{14.14}$$

The boundary condition at the water surface is $c = 0$, which is consistent with equation (14.8).

The evolution of the bed over time is calculated from the sediment continuity equation:

$$\frac{\partial \eta}{\partial t} = -\frac{1}{c_b}\left(\frac{\partial q_s}{\partial x} + \frac{\partial q_s}{\partial y}\right) \tag{14.15}$$

where η is the bed elevation. The sediment discharge, q_s, is the sum of the sand transported by bedload and in suspension. The suspended sand discharge is determined by vertically integrating the product of the flow velocity and the sand concentration.

The bedload is determined by applying the Meyer-Peter and Müller (1948) formula modified with the critical shear stress of the given grain size in place of their constant of 0.047:

$$\phi = 8(\tau_* - \tau_{*c})^{3/2} \tag{14.16}$$

where ϕ is the nondimensional bedload transport ($\phi = q/[(\rho_s/\rho - 1)gd^3]^{0.5}$), τ_* is the nondimensional boundary shear stress ($\tau_* = \tau/[(\rho_s - \rho)gd]$), and τ_{*c} is the nondimensional critical shear stress ($\tau_{*c} = \tau_c/[(\rho_s - \rho)gd]$). The grain diameter is represented by d; d_{50}, the median grain diameter, is used in the model results presented later. The density of the sand is represented by ρ_s.

The boundary shear stress used in equation (14.16) is the magnitude of the vector sum of the shear stress calculated from the flow equations and an apparent stress due to gravity. The apparent stress due to gravity is calculated with a method proposed by Nelson and Smith (1989a) in which

$$\tau_g = \tau_c \frac{\sin \xi \nabla \eta}{\sin \phi |\nabla \eta|} \tag{14.17}$$

where τ_g is the apparent gravitational stress, ξ is the local maximum bed slope, and ϕ is the grain angle of repose. The x and y components of the bedload are determined from the respective components of the flow velocity and components of the local bed slope. The magnitude of τ_g is zero where the bed is horizontal, and approaches τ_c where deposition increases the bed slope to the grain angle of repose.

A large fraction of the total shear stress at the bed is exerted as form drag on large roughness elements, such as the extreme irregularity of the bedrock channel, bedforms, and boulder-size talus and bed material. This form drag must be deducted from the total shear stress to arrive at the skin friction portion of the total shear stress that transports sediment. Wiele *et al.* (1996) calculated the fraction of the total shear stress active in transporting sediment in reaches of the Colorado River in the

vicinity of the reaches in this study. They made their calculation by determining the skin friction required to match measured transport rates during periods in which the sand supply was stable. This calculation yielded a skin friction that was 15% of the total shear stress. This low value is consistent with the extremely large channel roughness and associated form drag and was used in the calculations in this study in areas of the reach where the sand depth is less than the bed roughness.

The procedure used in this study for determining the skin friction in portions of the channel where the sand is sufficiently thick to cover the bed roughness is different from the one used by Wiele *et al.* (1996). Sand thickness tends to be greatest in recirculation zones, which are isolated from the tumultuous flow in the main channel, and where the flow and sand transport more closely resemble that of alluvial streams. In this region, the local channel resistance and skin friction were calculated as functions of local flow, depth and sand size. This procedure used the methods described by Bennett (1995) to estimate bedform dimensions and form drag. Bennett drew on the work of van Rijn (1984) who used u_* to distinguish between ripples, dunes and upper plane bed and to estimate the dimensions of the bedforms, if present. Given bedform height and wavelength, the local friction and skin friction are determined in Bennett's algorithm using the relations of Smith and McLean (1977) and Nelson and Smith (1989b). Relating local flow resistance and skin friction to bedforms is an improvement over the use of values derived only from the local hydraulics, but errors may be induced by uncertainties in the relations used and in the assumption of equilibrium between the local flow and the bedforms.

The model has been used to examine depositional processes and rates in the Colorado River main stem during a flood on the Little Colorado River (Wiele *et al.*, 1996), to examine the effect of sand supply on depositional patterns and magnitudes, and to compare the effects of natural tributary flooding with flooding caused by increased dam releases (Wiele, 1997; Wiele *et al.*, 1999). The model has shown good agreement with cross-section measurements from before and after the Little Colorado River flood in 1993 (Wiele *et al.*, 1996) and has replicated depositional patterns during the 1996 test flow (Wiele *et al.*, 1999). In one of the study reaches during the Little Colorado River flood, high sand concentrations led to massive deposition in the main channel (up to 12 m) and formed a large bar along the left side of the main channel in the recirculation zone. In contrast, with lower concentrations and higher water discharge during the test flow, the main channel scoured, and the focus of the deposition was near the recirculation zone reattachment point. The model replicated these differences in depositional pattern with no calibration. The accuracy of the model without calibration in these studies supports the use of the model to predict results for the hypothetical cases in this study.

14.3 Study site selection and morphology

Four modelling sites (Figure 14.1) were selected, which are within the study area of Hereford *et al.* (1991, 1993). Each of these reaches also contains gullies studied by Thompson and Potochnik (2000). The modelling site farthest downstream, the Upper Unkar reach, contains an especially sensitive archaeological site with abundant artefacts concentrated in a small area.

Debris flows and floods from streams in side canyons (Howard and Dolan, 1981; Schmidt, 1987; Webb *et al.*, 1989; Schmidt and Graf, 1990; Melis *et al.*, 1994; Schmidt and Rubin, 1995) form debris fans that partially constrict the channel, and recirculation zones are generated in the lee of the channel constriction. The spacings between debris fans are controlled to a large degree by bedrock structure (Dolan *et al.*, 1978). The bed of the Colorado River in Grand Canyon National Park is about 60% bedrock, talus blocks or boulders. Sand supplied to the mainstem river by tributary floods is stored primarily along the channel sides and in recirculation zones. Sand is stored temporarily on the channel bottom (Howard and Dolan, 1981; Wilson, 1986; Schmidt and Graf, 1990).

The four study reaches discussed in this report are located between 112 and 140 km below the dam, starting about 6 km downstream from the confluence with the Little Colorado River (Figure 14.1), one of the two main sand-supplying tributaries. The reaches modelled in previous studies tended to have narrow constrictions with large, abrupt expansions that produced large, well-developed recirculation zones. These large zones can be effective at storing large volumes of sand. Reaches modelled in this study have channel constrictions and recirculation zones, but the expansions are narrower or more constrained and the resulting recirculation zones are smaller than the previously modelled reaches. In the two downstream reaches in this study, the recirculation-zone sand deposits are less significant than the channel-margin deposits. To clarify the discussion and to avoid repeated, lengthy descriptions of morphological features in the reaches, these features are designated with letters in the accompanying figures.

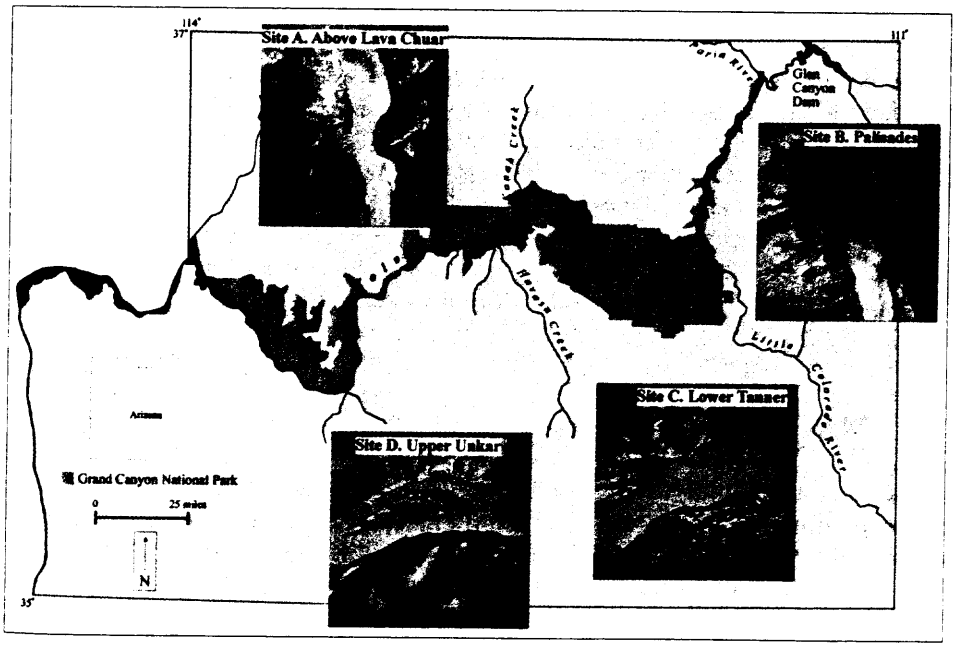

Figure 14.1 *Aerial photos of study sites and map showing study site locations.*

14.4 Model grids

Channel bathymetry was measured in the study reaches by the Grand Canyon Monitoring and Research Center (GCMRC). A fathometer mounted on a manoeuvrable boat recorded local water depth. The location of the fathometer, including elevation, was tracked from a shore station with a theodolite manually trained on a target mounted directly above the fathometer. The boat followed streamwise and cross-stream lines spaced about 10 m apart (see Andrews *et al.*, 1999, for a more detailed description of surveying methods). In addition, the shoreline was surveyed to outline channel shape; additional measurements were made around and over sand deposits (Figure 14.2).

The water discharge was about 425 m^3/s during the measurements of channel shape. In order to form topographic maps that extend to elevations in excess of the river stage at 2830 m^3/s , the field-surveyed bathymetric and shoreline data were combined with GCMRC photogrammetrically generated contour data (Figure 14.2). Where the data sets overlapped, which typically occurred near the channel margin, the field-surveyed data were used to generate the topographic surface because these data were considered to be more accurate. A Triangulated Irregular Network (TIN) surface model was created using the Delauney method of triangulation in which topographic features are developed into a series of connected triangles where the nodes of the triangles correspond to measured locations and the facets of the triangles correspond to changes in slope. Contours were generated from the TIN surface and corresponded well with the photogrammetric contours in the areas of overlap. The TIN surface was then interpolated using a bivariate quintic interpolation scheme, implemented by the ARC/INFO Geographical Information System software (Environmental Systems Research Institute, Inc., 1991), in order to generate 10-m resolution grids used as the basis for model calculations (Figure 14.3).

The choice of grid spacing requires a balance between computational efficiency, especially given the demands of a time-stepping model, and sufficient detail. The 10-m grid is sufficient for computing sand volumes and locations, but does not capture metre-scale detail such as backwater channels. Comparisons with model results using a 5-m grid showed smoother representation of channel shape, but provided no significant improvement on calculated volumes. Tighter grids are more compatible with the calculation of flow fields only, without time-stepping erosion and deposition, and can be helpful for some applications such as habitat studies (e.g. Korman *et al.*, 2004).

14.5 Model application and results

In addition to channel shape, application of the model requires specification of discharge, downstream water surface elevation at that discharge, sand flux and grain size into the reach, and the initial thickness of sand deposits. Two water discharges were modelled in this study: 1270 m^3/s, corresponding to the 1996 test flow, and 2830 m^3/s, which is close to the pre-dam average annual flood and the highest discharge (in 1983) since the closure of Glen Canyon Dam in 1963. Three sand conditions (Figure 14.4) were modelled in each reach. These sand conditions are

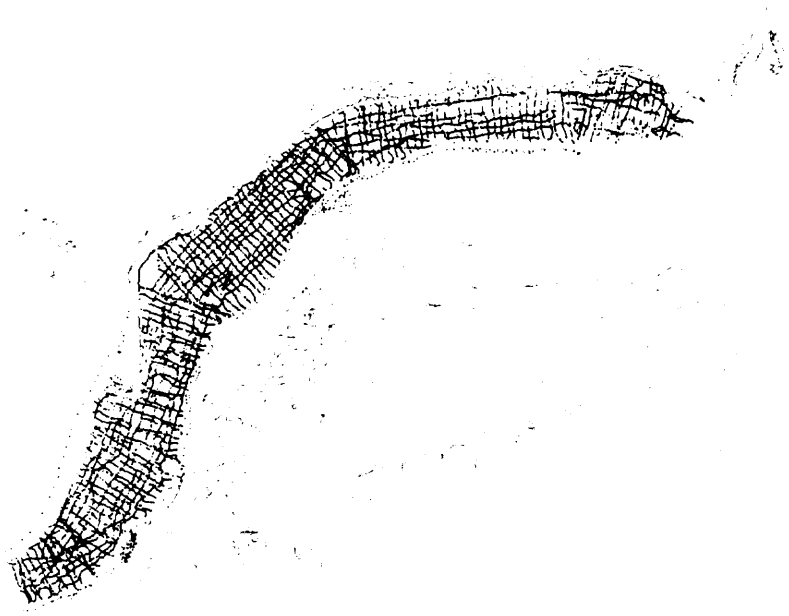

Figure 14.2 *Illustration of the Lower Tanner reach showing the locations of the field-surveyed bathymetric and shoreline surveys (dots in the main channel and along the channel sides) combined with GCMRC photogrammetrically generated contour data.*

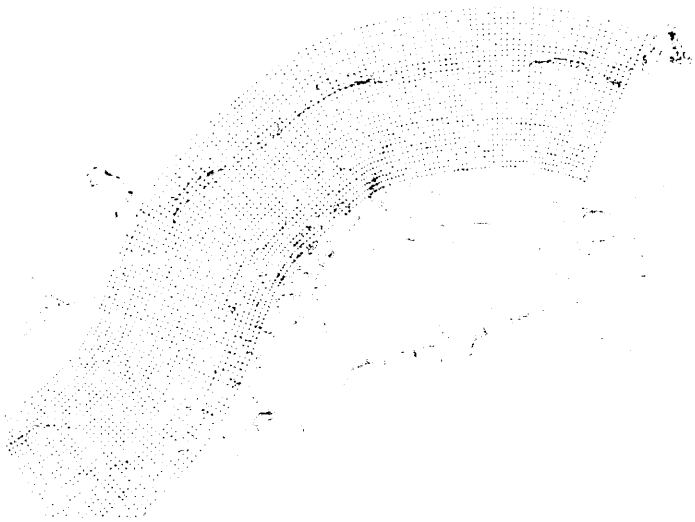

Figure 14.3 *Computational grid (dots) of the Lower Tanner reach superimposed on the topography. Elevations at the grid points are interpolated from the TIN surface.*

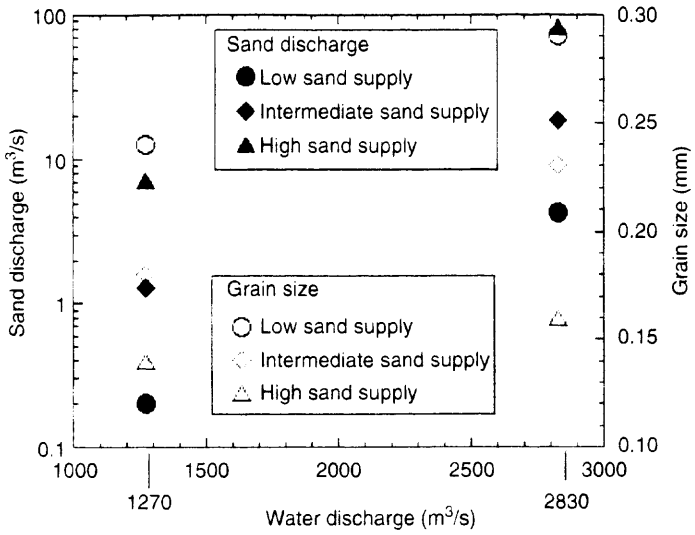

Figure 14.4 *Sand discharge and grain size as functions of water discharge for three sand conditions used as boundary conditions for the model runs: high sand supply during 1956, intermediate sand supply represented by the conditions during the 1996 test flow and low sand supply during 1983. These values for sand discharge and grain size were contributed by Topping (USGS, written communication, 1998).*

representative of historical high sand supplies, historical low sand supplies and an intermediate condition corresponding to that which occurred during the 1996 test flow. The historical high sand supply corresponds to conditions represented by measurements in 1956, prior to the dam construction. The historical low was taken from sand conditions in 1983, after the dam had been eliminating main channel inputs for nearly 20 years and during flows approaching 2830 m^3/s. These two conditions, high discharge and low sediment supply, combined to winnow the bed to a coarser state and thereby reduce suspended sand transport (Topping *et al.*, 2000a,b). The 1996 sand conditions are representative of typical contemporary conditions. The upstream sand boundary conditions corresponding to the three sand supplies were taken from sand rating curves supplied by David J. Topping (US Geological Survey, written communication, 1998). Topping (1997) related sand concentrations and sand sizes to antecedent conditions and the evolving status of sand on the channel bed, which forms the source from which sand in suspension is derived.

One of the initial conditions that must be specified is the sand coverage on the bed at the start of the simulation. Previous model applications have been in reaches in which bathymetric measurements have been repeated, allowing for the estimation of a minimum bed elevation by combining the lowest elevations from different surveys. Another approach in modelling events in which the change in sand deposits is dominantly depositional, and where there is insufficient information to synthesize a minimum bed elevation, is to neglect erosion and make the starting bed shape the minimum bed elevation. In this study, the local initial sand conditions on the bed were estimated by running the model in each reach at a discharge characteristic of dam operation (481 m^3/s was chosen for these simulations) with a sand boundary

condition at the inlet appropriate for the discharge and sand supply. The model was run until the sand coverage reached near-equilibrium with the sand influx. For the cases with low and intermediate sand supply, corresponding sand boundary conditions were used to model the initial sand coverage. The highest sand supply, however, is produced by relatively brief events (David J. Topping, US Geological Survey, oral communication, 1999), such as local tributary flooding. As a result, a bed in equilibrium with the intermediate sand supply was judged a more reasonable antecedent condition for the high sand supply than a bed configuration in equilibrium with the high sand supply.

The effects of the different combinations of water and sand discharge on sand deposition are considered in the following sections. The final results are taken from the end of the simulation. The length of the simulation varies as a result of differences in the real time required for the model run. The length of the model runs depends on the time step, which is determined within the model on the basis of the rate at which deposition or erosion occurs. As a result, events with rapid changes in bed morphology, such as would occur with the high sand supply, generally progress in the model much more slowly in real time than events in which there is little change in bed morphology. Nevertheless, direct comparisons between model results under different conditions can be made at different times because most of the changes within a reach occur rapidly. The events with the shortest elapsed simulation time (as a result of small time steps causing slow rates of advance in time) tend to be those with the most rapid changes and, therefore, reach near-equilibrium in the least amount of simulated time.

Although maximum sand deposition is generally favourable for the restoration and preservation of the riparian environment, deposition within the main channel is of little long-term value because the sand storage is short-lived. Reduction in sand supply, by the cessation of tributary flooding (which is the only mechanism currently capable of producing high sand concentrations), will lead to the rapid erosion of main channel deposits. For the purposes of this study, we emphasize near-shore environments and deposits above the 708 m^3/s stage. In the two upstream reaches, most of the deposition that would be likely to fill gully mouths occurs in recirculation zones, and so these environments are considered in detail. In the two downstream reaches, in which deposition is not dominated by recirculation zones, deposits along the channel sides above the 708 m^3/s stage are considered. The depositional patterns and volumes with the intermediate sand supply are generally bracketed by the results with the high and low sand supplies. Consequently, only the model predictions with the high and low sand supplies are shown in the figures.

14.6 The four modelling sites

14.6.1 Above Lava Chuar reach

14.6.1.1 Initial conditions

The Above Lava Chuar reach contains an expansion along river left (i.e. left side of the river looking downstream) in the upper part of the reach (A) that shows no

recirculation at either 1270 (Figure 14.5a) or 2830 m^3/s (Figure 14.6a). The debris fan at the downstream end of this expansion (B), however, generates a small recirculation zone in the embayment (C) formed between it and another debris fan (D) immediately downstream. The downstream debris fan (D) also partly forms the Lava Chuar rapid. The bank along river right consists of a steep cliff along most of its length; a side channel forms an indentation (E) about 500 m from the reach inlet and a camping beach (F) is at the downstream end of the bank. Gullies mapped by Hereford *et al.* (1991, 1993) appear in two locations in the Above Lava Chuar reach, in the vicinity of B and D and downstream from F. The greatest concentration is in C, and two gullies reach the water level in F.

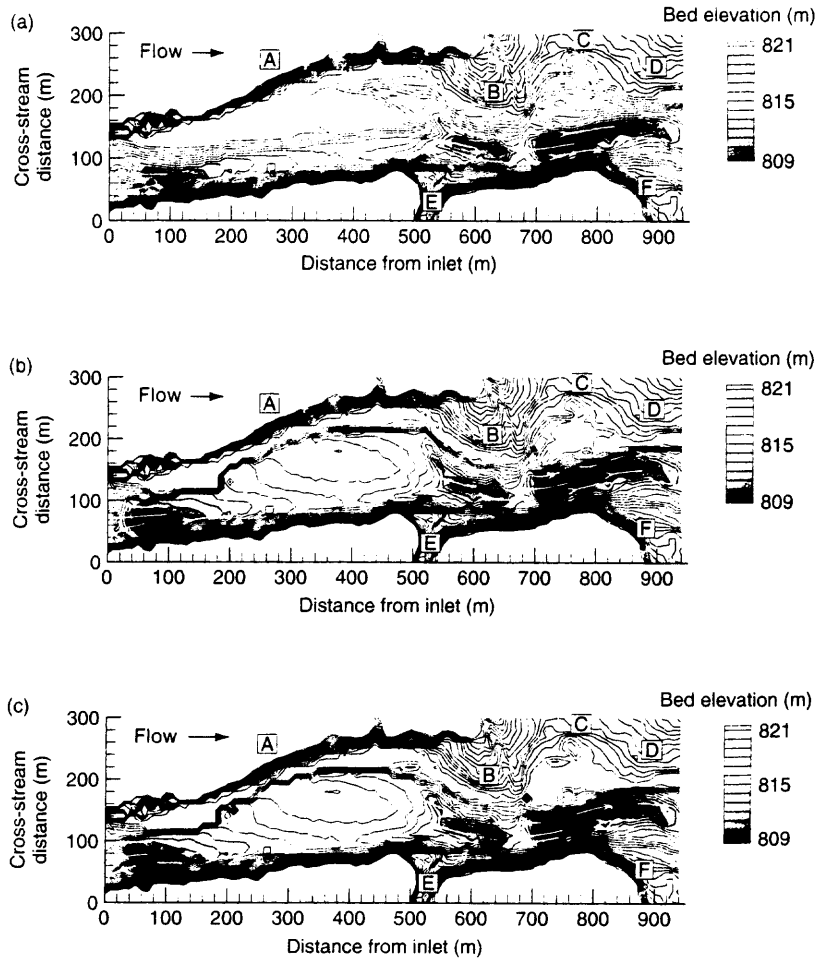

Figure 14.5 *Contour maps of the Above Lava Chuar reach at 1270 m^3/s showing (a) the initial bed morphology (at time = 0), (b) the model prediction after 72 hours with the low (1983) sand supply and d_{50} = 0.24 mm, and (c) the model prediction after 68 hours with the high (1956) sand supply and d_{50} = 0.16 mm.*

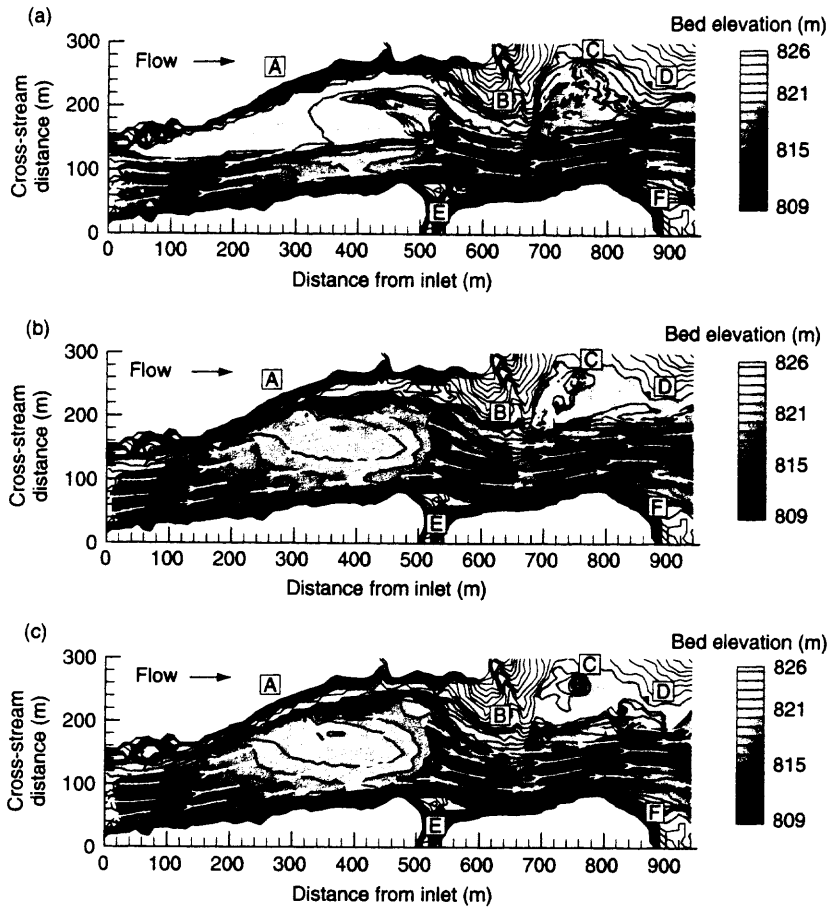

Figure 14.6 *Contour maps of the Above Lava Chuar reach at 2830 m^3/s showing (a) the initial bed morphology (at time = 0), (b) the model prediction after 72 hours with the low (1983) sand supply and d_{50} = 0.29 mm, and (c) the model prediction after 37 hours with the high (1956) sand supply and d_{50} = 0.14 mm.*

14.6.1.2 Model predictions

The total change in sand deposit volume in the Above Lava Chuar reach was negative for all cases (Figures 14.5, 14.6 and 14.7) largely as a result of erosion of the sand deposit in the channel expansion marked A under all combinations of discharge and sand supply (Figure 14.8). The modelled erosion of the sand bar in A may, in part, be a consequence of the model's functioning with just one grain size. If the initial sand deposit within the expansion were of significantly coarser material than the modelled grain size, it would be more resistant to erosion. The combination of high discharge and finest grain-size resulted in the most rapid erosion (Figure 14.8). During the course of this erosion, bars that deflect flow towards the bank formed within the expansion, resulting in erosion of sand deposits along the bank. After the

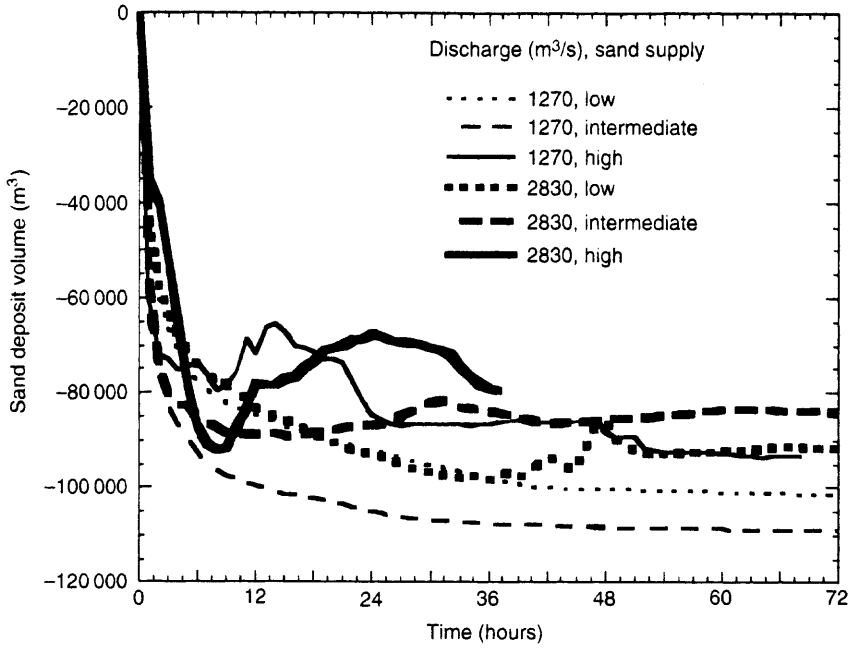

Figure 14.7 *Modelled change in sand volume as a function of time in the Above Lava Chuar reach.*

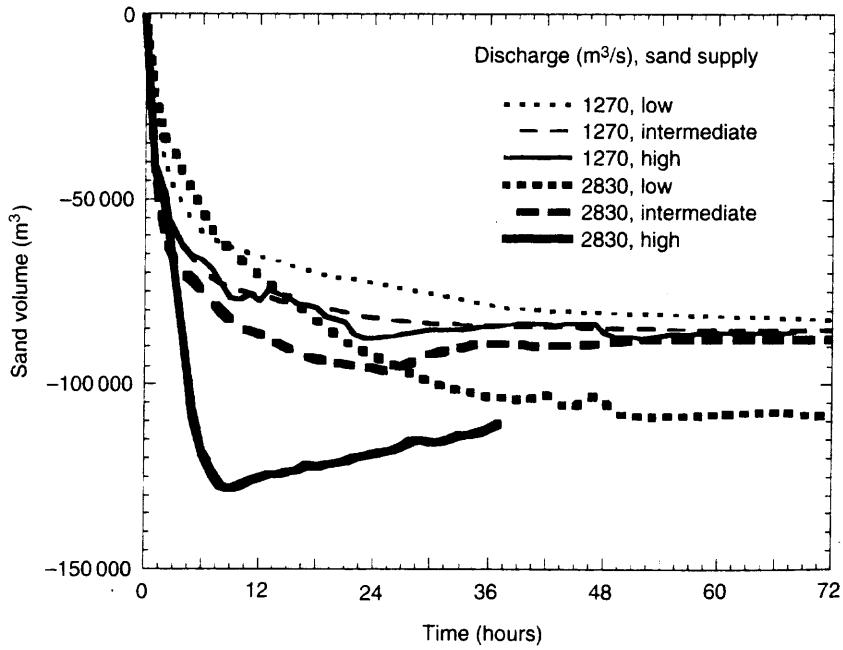

Figure 14.8 *Modelled change in sand volume as a function of time at location A in the Above Lava Chuar reach.*

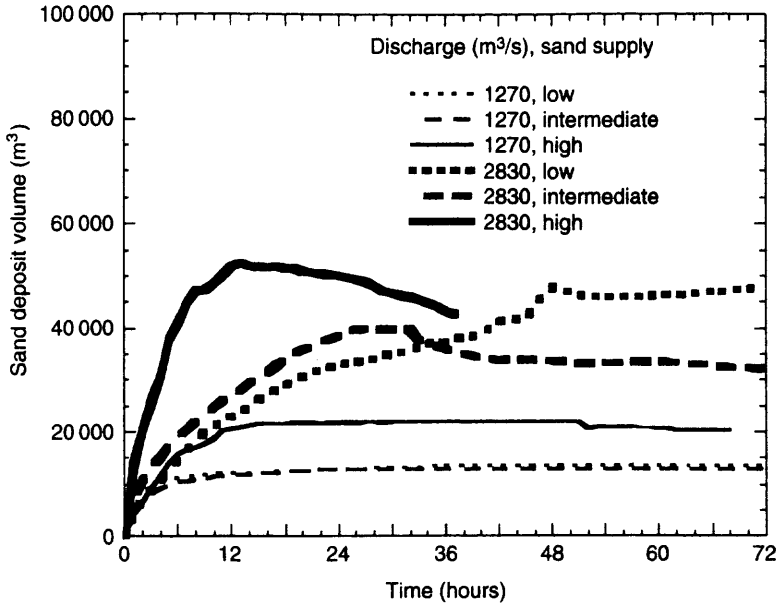

Figure 14.9 *Modelled change in sand volume as a function of time at location C in the Above Lava Chuar reach.*

bars migrated downstream, the sand deposits in A were restored slightly as sand was redeposited along the bank.

Deposition occurred in all cases within C (Figures 14.5, 14.6 and 14.9), the most critical area for archaeological resources. The sand volume within C increased with higher sand concentration in the flow at 2830 m^3/s during the first day (Figure 14.9). There was a rapid initial increase in sand volume, followed by a steady decline after about 12–14 hours. This pattern is related to the increase in sand flux that resulted from the erosion of the sand deposit in A, followed by partial erosion of the deposit in C after most of the sand in A had been evacuated. A similar pattern, but with a smaller amplitude, occurs for the intermediate sand supply. At 1270 m^3/s, model results show volumes similar to the low and intermediate sand supplies, and the largest sand volume coincided with the high sand supply. At 2830 m^3/s, more sand was deposited within the embayment and to a higher elevation, although backwaters remained in the embayment.

14.6.2 Palisades reach

14.6.2.1 Initial condition

The Palisades reach has a simpler form than the Above Lava Chuar reach, with a recirculation zone (G) on river left downstream from the rapid that forms the reach inlet (Figures 14.10a and 14.11a). The channel expands (H) downstream from the recirculation zone. A cobble bar is located midway in the channel adjacent to H

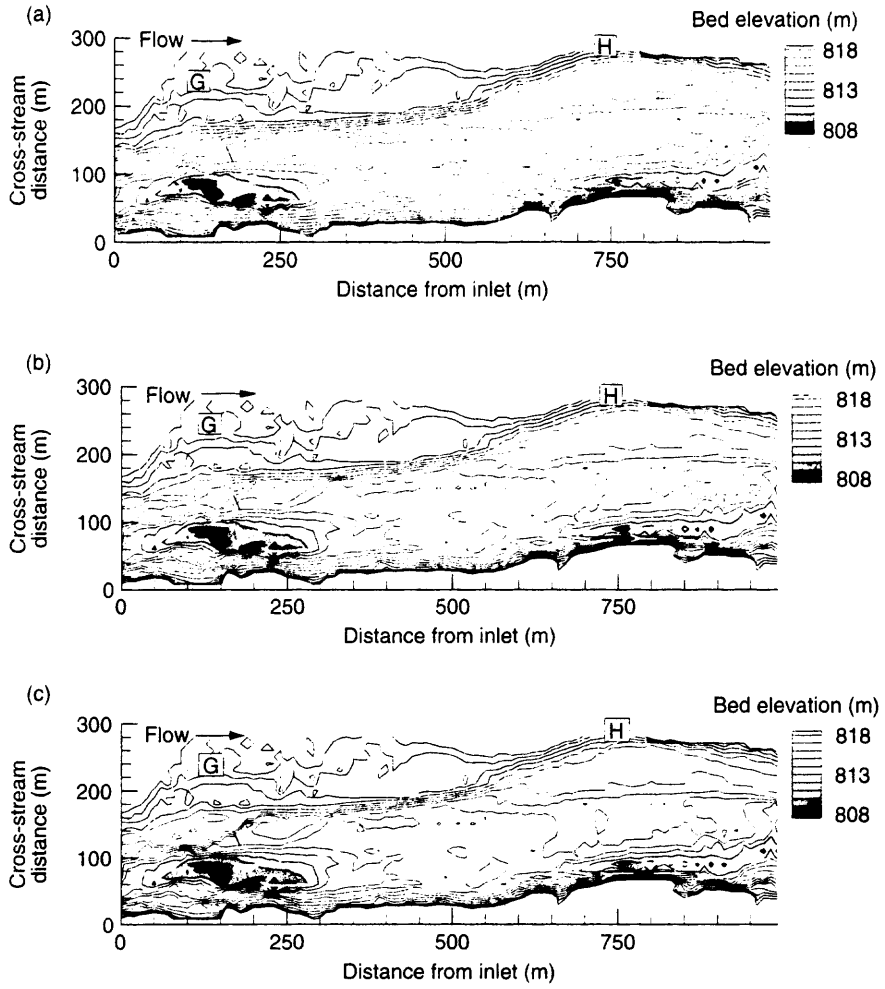

Figure 14.10 *Contour maps of the Palisades reach at 1270 m³/s showing (a) the initial bed morphology (at time = 0), (b) the model prediction after 72 hours with the low (1983) sand supply and* d_{50} *= 0.24 mm, and (c) the model prediction after 72 hours with the high (1956) sand supply and* d_{50} *= 0.16 mm.*

where the thalweg is close to the right bank. The deepest part of the channel is downstream from the inlet near the centre of the channel. The right bank consists of a cliff along most of its length.

Gullies mapped by Hereford *et al.* (1991, 1993) in this reach are near G. The gently sloping surface above G contains many artefacts (Yeatts, 1996; K. Thompson and A. Potochnik, SWCA, oral communication, 1999). The gullies within G in the Palisades reach have a lower gradient and appear less deeply incised than gullies in the Above Lava Chuar reach. If further incision of gullies is to be arrested or past incision healed by deposition along the water's edge, these sites may be the best candidates for benefits from high releases.

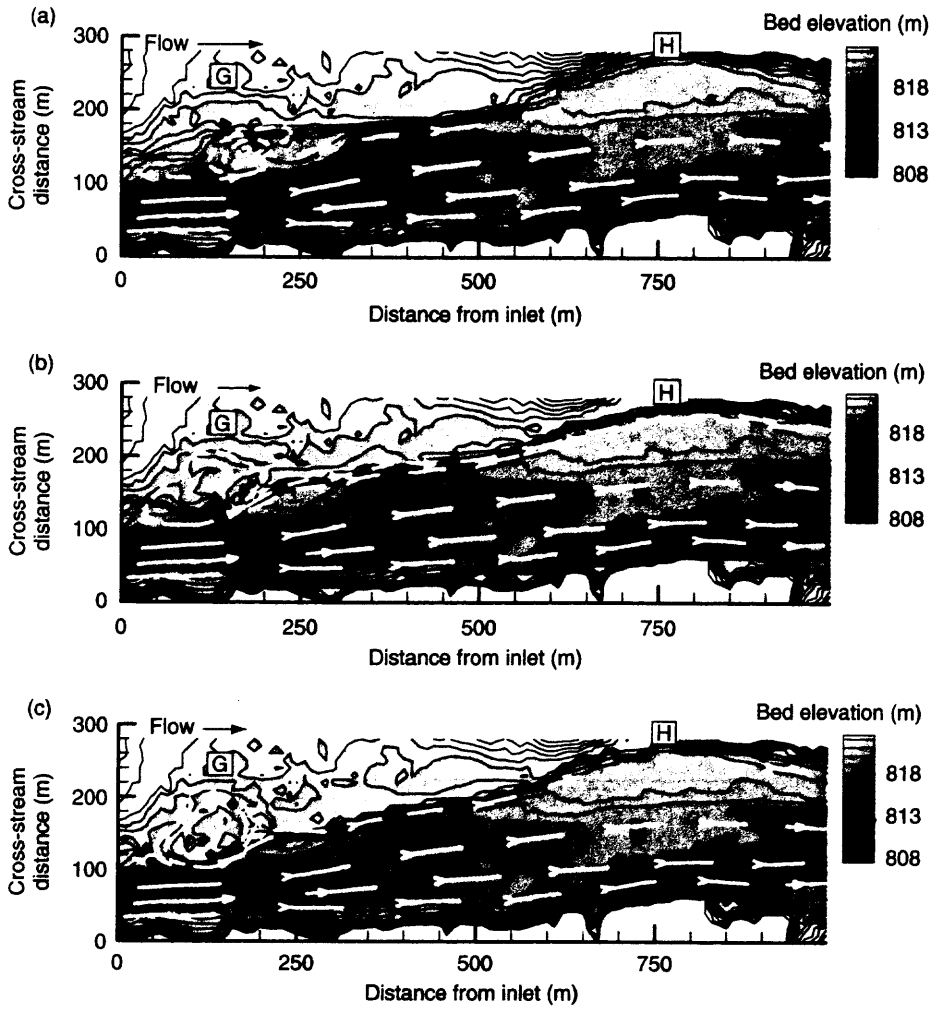

Figure 14.11 *Contour maps of the Palisades reach at 2830 m³/s showing (a) the initial bed morphology (at time = 0), (b) the model prediction after 72 hours with the low (1983) sand supply and d_{50} = 0.29 mm, and (c) the model prediction after 31 hours with the high (1956) sand supply and d_{50} = 0.14 mm.*

14.6.2.2 Model predictions

The most important depositional site in the Palisades reach is G, the recirculation zone on river left near the reach inlet. Hereford *et al.* (1991, 1993) mapped gullies extending to the 142 m^3/s water surface in this area. Modelling results (Figures 14.10, 14.11 and 14.12) show that some deposition will occur in G under all combinations of water discharge and sand conditions. The initial deposit volume increased with the amount of sand available for transport at 2830 m^3/s, and the volumes were larger for all cases at 2830 m^3/s than at 1270 m^3/s (Figure 14.13). At 1270 m^3/s with the low sand supply, minimal deposition occurred in G, and most of that extended upstream from the

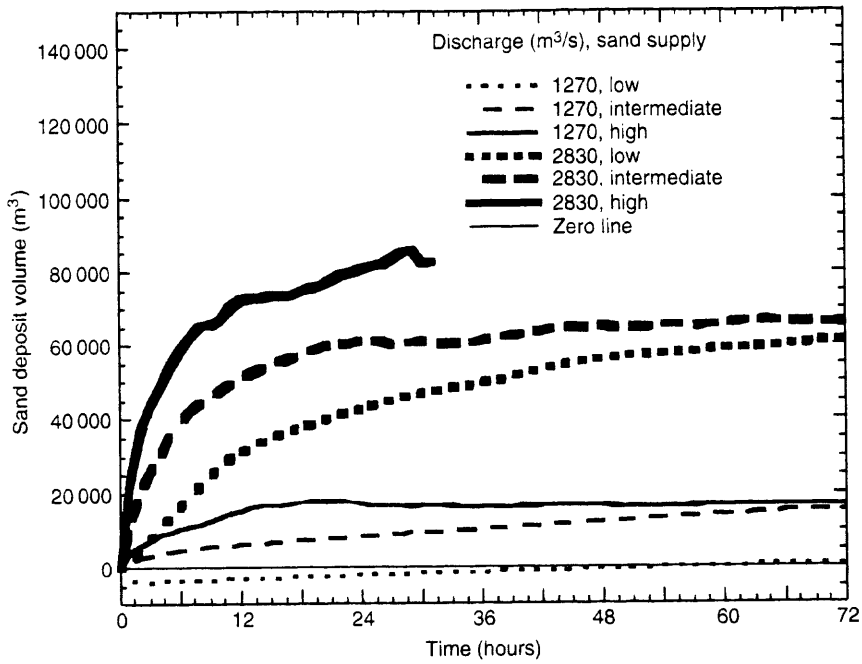

Figure 14.12 *Modelled change in sand volume as a function of time in the Palisades reach.*

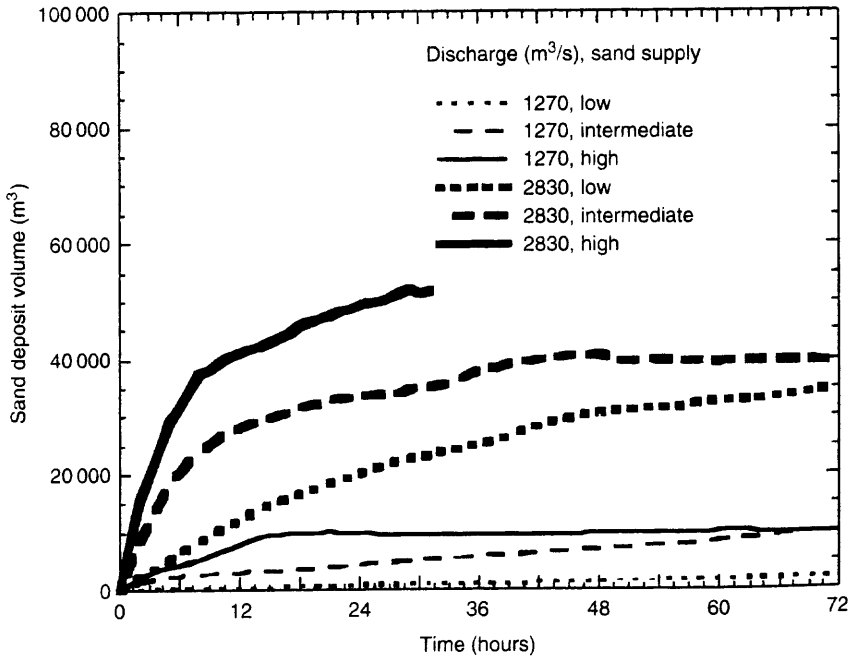

Figure 14.13 *Modelled change in sand volume as a function of time at location G in the Palisades reach.*

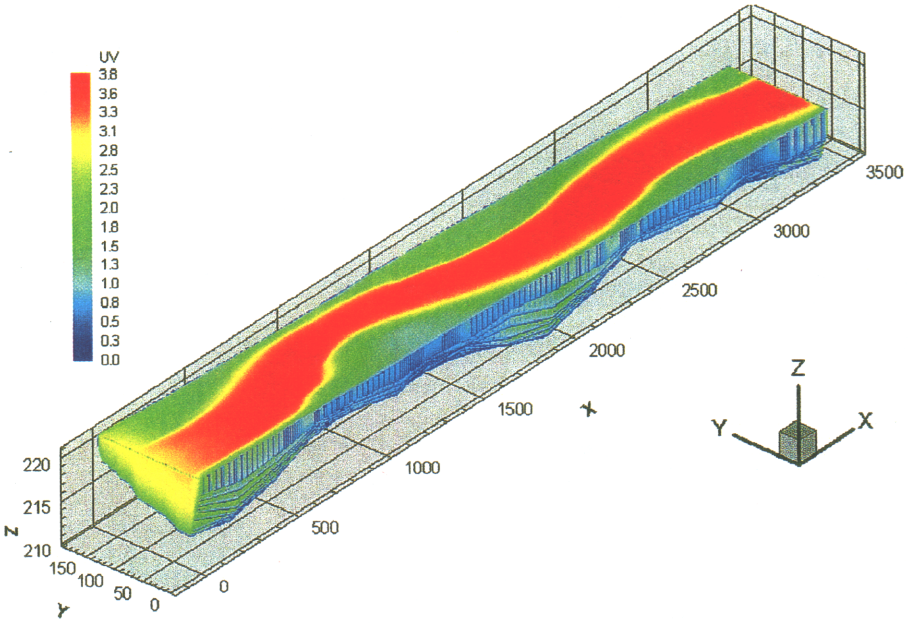

Plate 1 (Figure 11.5) Scalar product of u and v velocities in ms^{-1} predicted by Stoesser *et al.* (2003) for the 3.5 km reach of the River Rhine shown in Figure 11.4. (Published by IWA Publishing.)

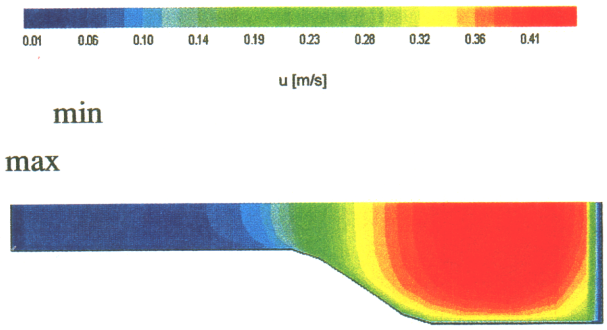

Plate 2 (Figure 15.15) See main text for caption.

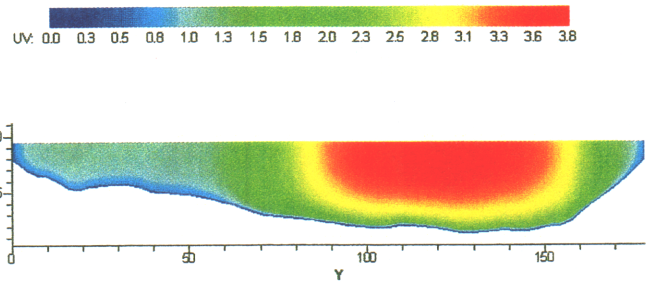

Plate 3 (Figure 15.20) See main text for caption.

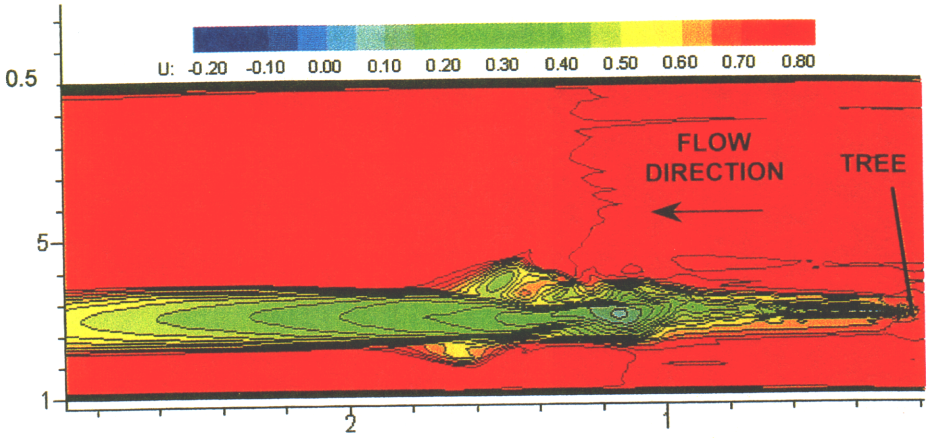

Plate 4 (Figure 15.16) Instantaneous velocity distribution, length unit for both axes in metres.

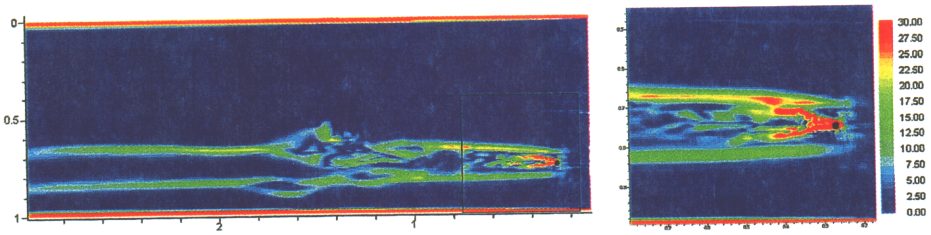

Plate 5 (Figure 15.17) Stress tensor distribution (in 1/s), length unit in metres.

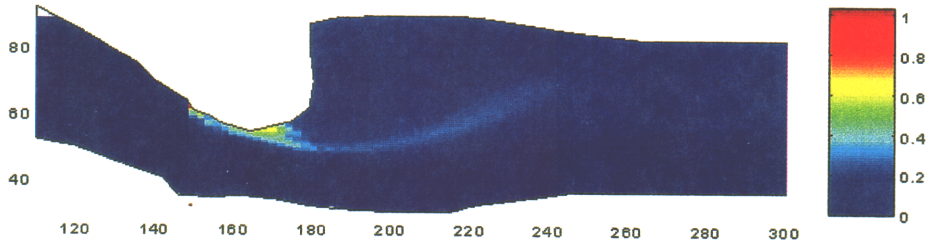

Plate 6 (Figure 17.6) Map of prediction bounds. The normalised weighted deviation from the mean concentration field as an indicative measure of risk that model predictions are more uncertain. A measure of 0 (dark blue) represents locations where there is little deviation between all the different model predictions, and a measure of 1 means there is a large deviation, which gives rise to wider prediction limits.

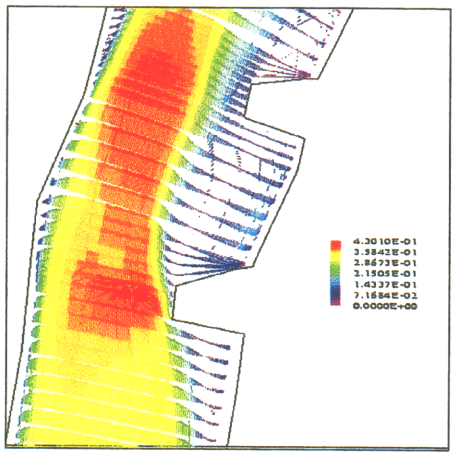

Plate 7 (Figure 18.11) Velocities 20% below surface at deflector 3f.

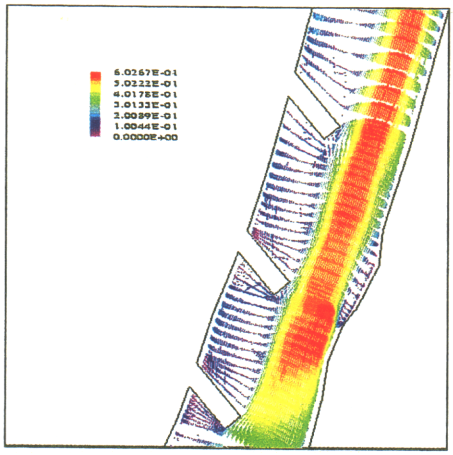

Plate 8 (Figure 18.12) Velocities 20% below surface at deflector 3c.

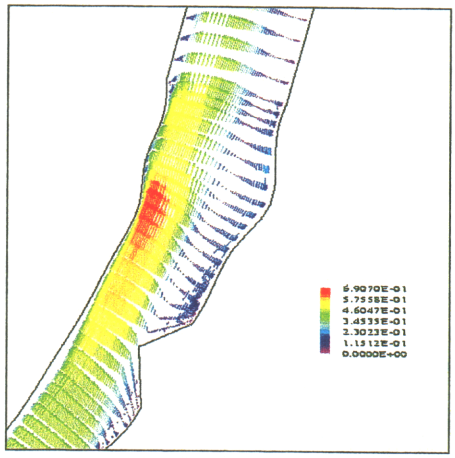

Plate 9 (Figure 18.13) Velocities 20% below surface at deflector 6a.

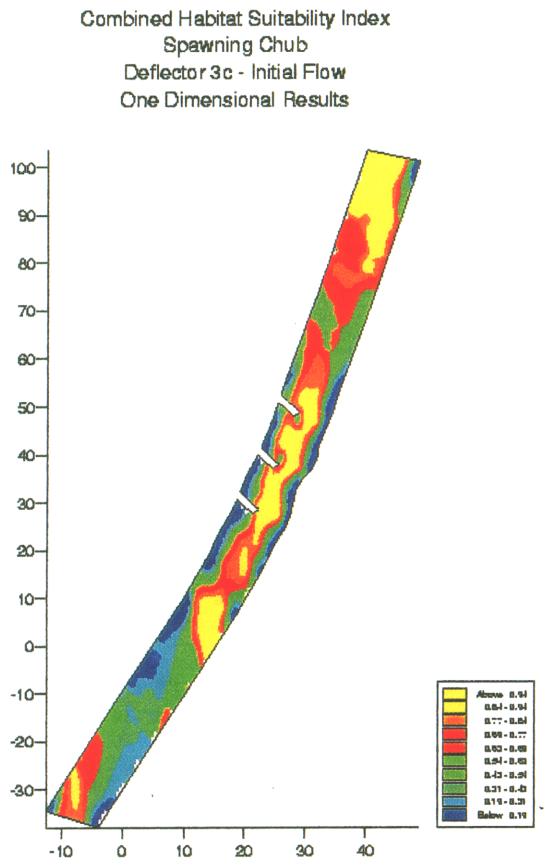

Plate 10 (Figure 18.14) Spatial Plots of WUA for spanning chub at deflector 3c for 1D model.

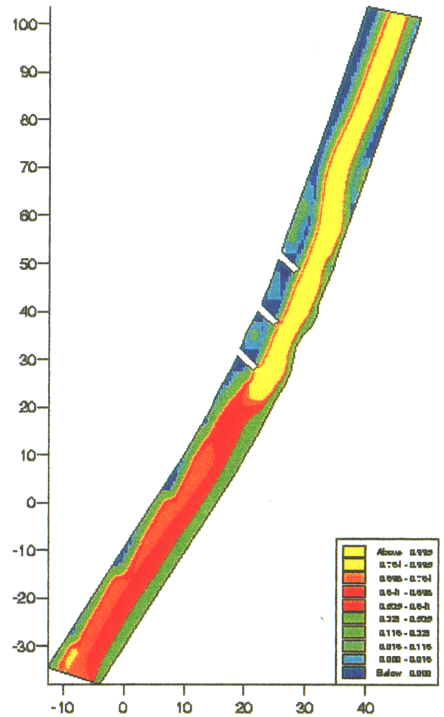

Plate 11 (Figure 18.15) Spatial Plot of WUA for spanning chub at deflector 3c for 3D model.

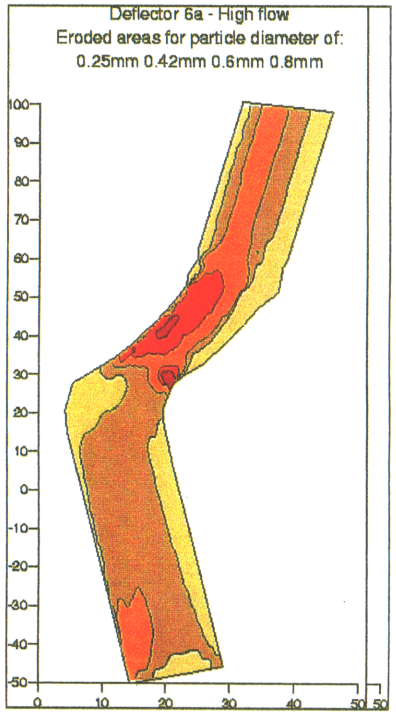

Plate 12 (Figure 18.18) Erosion patterns for different grain sizes.

reattachment point; deposition in the region of the gully mouths was less than in all other cases. The intermediate and high sand supplies at 1270 m^3/s produced deposits better suited to archaeological site preservation because deposition was greatest close to the water's edge. With the intermediate sand supply, sand accumulated at a steady rate over the course of the simulation and the volume matched the sand volume obtained with the high sand supply by the end of the simulation. With the high sand supply, however, most of the accumulation occurred within the first 14 hours. All three cases at 2830 m^3/s deposited more sand than the 1270 m^3/s cases, and the deposit volume increased with increased sand supply. Most of the deposition was near the reattachment point and along the cobble bench that forms the left bank at the 2830 m^3/s stage.

14.6.3 Lower Tanner reach

14.6.3.1 Initial conditions

The Lower Tanner reach (Figures 14.14a and 14.15a) is unlike the Above Lava Chuar and Palisades reaches in several respects. The Lower Tanner reach is longer (about 1200 m), has significant curvature and does not contain a large recirculation zone that dominates the sand storage in the reach. The outside of the bend, along river right, is bordered by bedrock cliffs along the upper half of the reach. The area near the outlet on river right consists of a low gravelly bench. The interior of the bend, along river left, is bounded by fans. Coppice dunes were mapped by Hereford

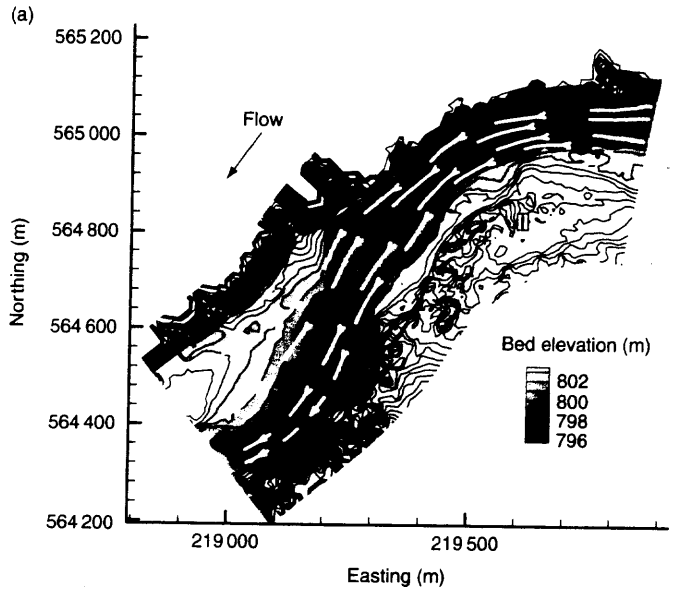

Figure 14.14 *Contour maps of the Lower Tanner reach at 1270 m^3/s showing (a) the initial bed morphology (at time = 0), (b) the model prediction after 72 hours with the low (1983) sand supply and d_{50} = 0.24 mm, and (c) the model prediction after 72 hours with the high (1956) sand supply and d_{50} = 0.16 mm.*

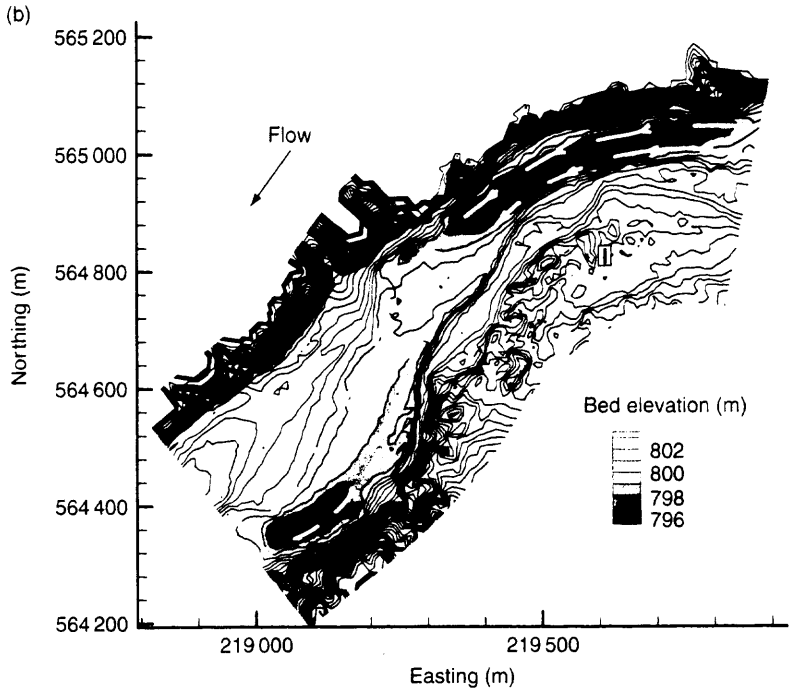

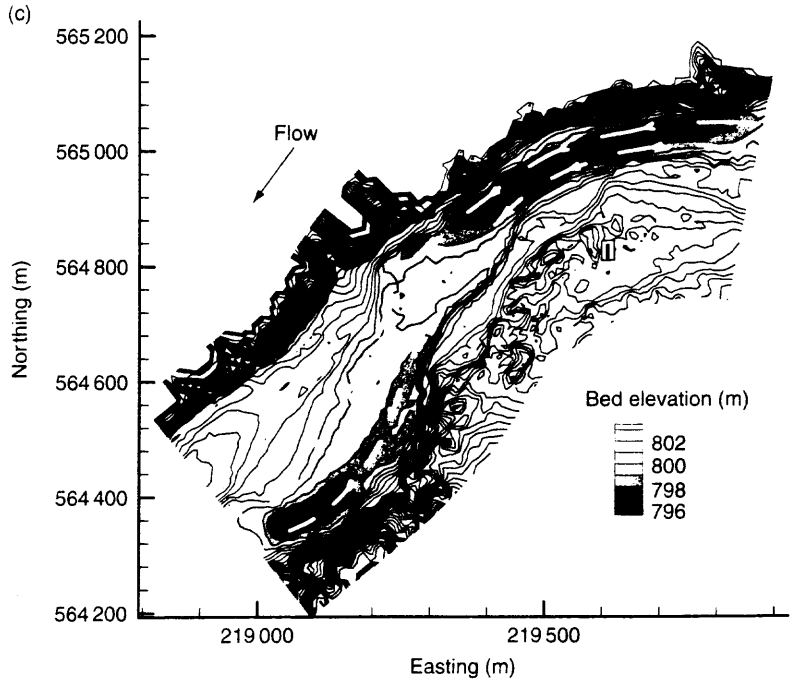

Figure 14.14 *(Continued).*

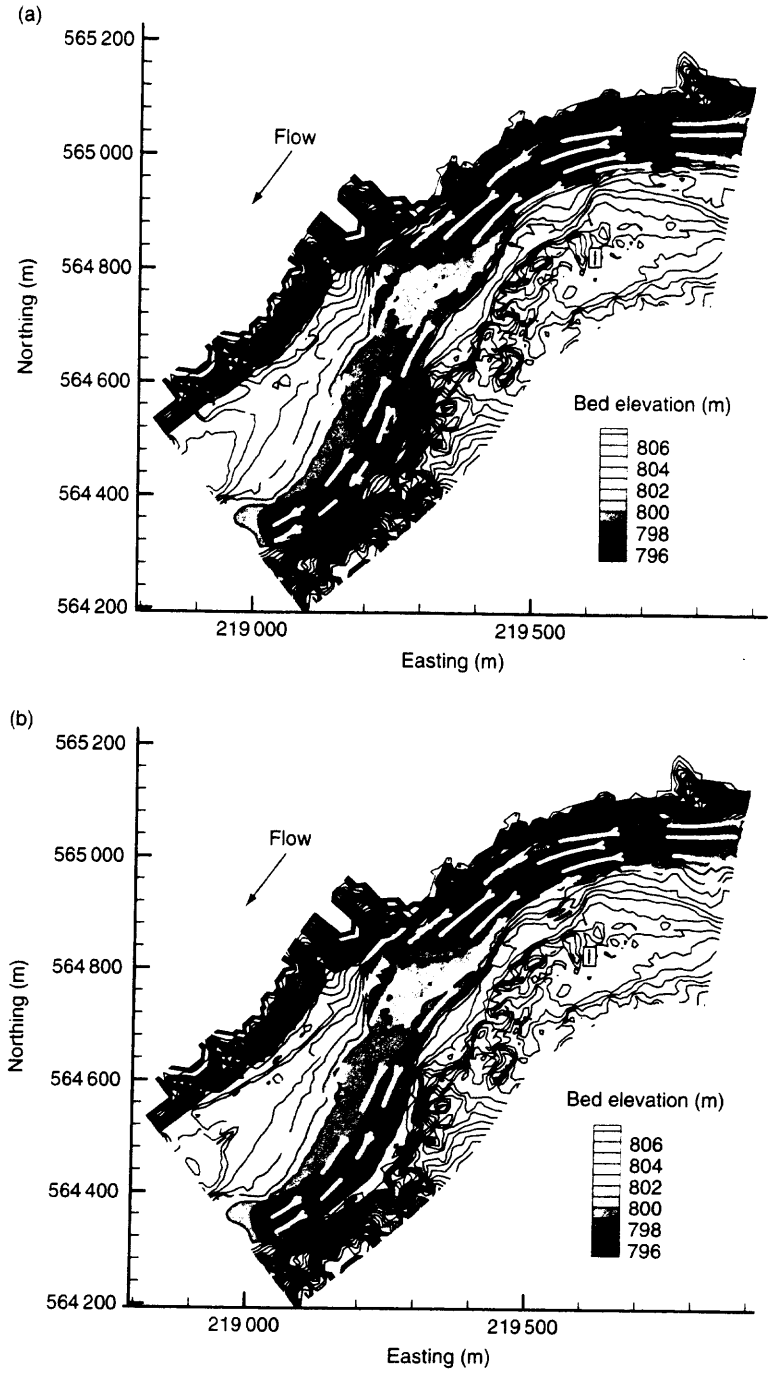

Figure 14.15 *Contour maps of the Lower Tanner reach at 2830 m^3/s showing (a) the initial bed morphology (at time = 0), (b) the model prediction after 72 hours with the low (1983) sand supply and d_{50} = 0.29 mm, and (c) the model prediction after 35 hours with the high (1956) sand supply and d_{50} = 0.14 mm.*

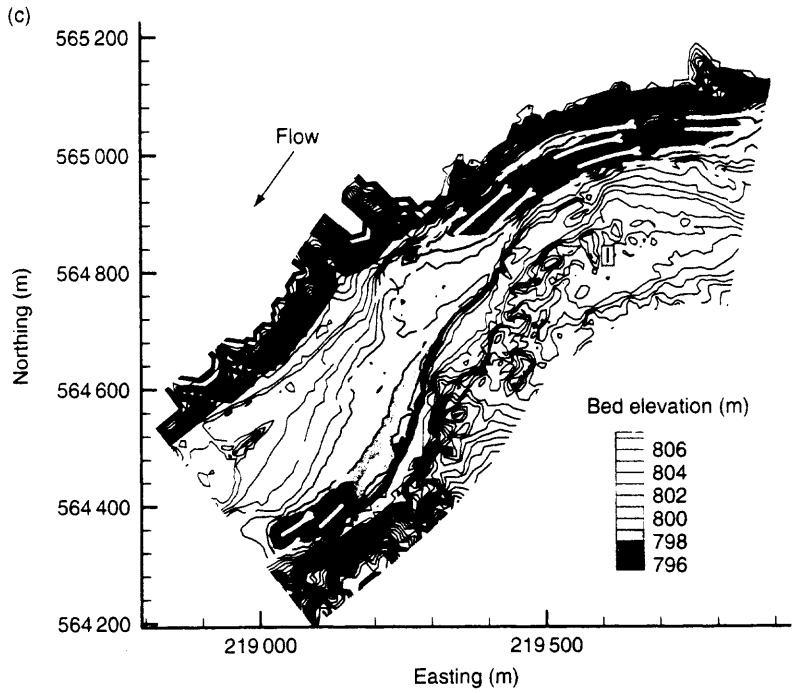

Figure 14.15 *(Continued).*

et al. (1991, 1993) in the area marked as "I" on Figures 14.14 and 14.15, and most of the gullies are contained in this area.

Most of the gullies mapped by Hereford *et al.* (1991, 1993) in this reach are on river left near the middle and downstream parts of the reach (Figures 14.14 and 14.15). Deposition predicted by the model was primarily along the channel sides, especially in the lee of bank irregularities that were too small to form well-developed recirculation zones. Deposition in the lee of bank irregularities may correspond to the deposition in microeddies proposed by John C. Schmidt (Utah State University, oral communication, 1999) as a significant depositional process, but eddies on the scale of the computational grid are represented in the model by the channel roughness.

14.6.3.2 Model predictions

Model predictions of deposition rates for the entire channel show a straightforward relation between sand supply and discharge and the consequent deposition (Figure 14.16). At both discharges, deposit volume increased with increased sand supply, and after 12 hours, the higher discharge produced larger deposits for all sand supplies.

At 1270 m^3/s, deposition rates for sand deposits above the 708 m^3/s stage follow similar patterns, asymptotically approaching a maximum value (Figure 14.17). The magnitude of the deposit volume is proportional to the sand supply at 1270 m^3 s. With the low and intermediate sand supplies, the maximum deposit volume is reached after about 48 hours, and only slight increases occur subsequently. With

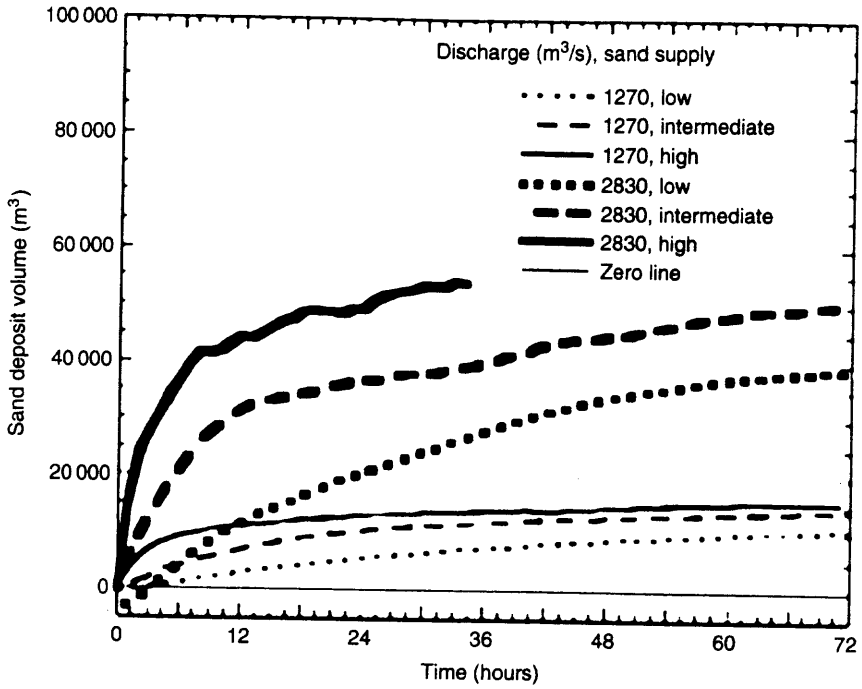

Figure 14.16 *Modelled change in sand volume as a function of time in the Lower Tanner reach.*

the high sand supply, the maximum value was reached after about 1 day. In contrast to the smoothly increasing deposit volume at 1270 m^3/s, sand deposits above the 708 m^3/s stage at 2830 m^3/s accumulated in irregular temporal patterns. The initial deposition rate was highest with the high sand supply, but dropped off after about 6 hours to match the sand volume accumulated with the intermediate sand supply. With the low sand supply, an initial scouring was followed by a rapid increase in volume until about 12 hours, followed by a steady increase in sand volume over the rest of the simulation. A sand deposit on river left near the reach inlet was inundated at 2830 m^3/s and eroded at that discharge with all sand supplies. With the low sand supply, deposition elsewhere was initially insufficient to offset erosion at this location. Sand volume at 2830 m^3/s with the low sand supply exceeded all the sand deposited at 1270 m^3/s after about 36 hours.

The volume of deposits above the 708 m^3/s stage, which have the most potential for preservation, is only about a third of the sand volume stored in the recirculation zone in the Above Lava Chuar reach (zone C) and the recirculation zone in the Palisades reach (zone G). This relatively small volume reflects the absence of significant recirculation zones in this reach. The volume of sand with preservation potential in this reach is small compared to that in the two upstream reaches, but there is some compensation in that these deposits are above typical dam-release stages. The recirculation deposits in the upstream reaches, although removed from the main channel, are subject to flow-induced erosion, albeit at a rate much lower than that for main channel deposits.

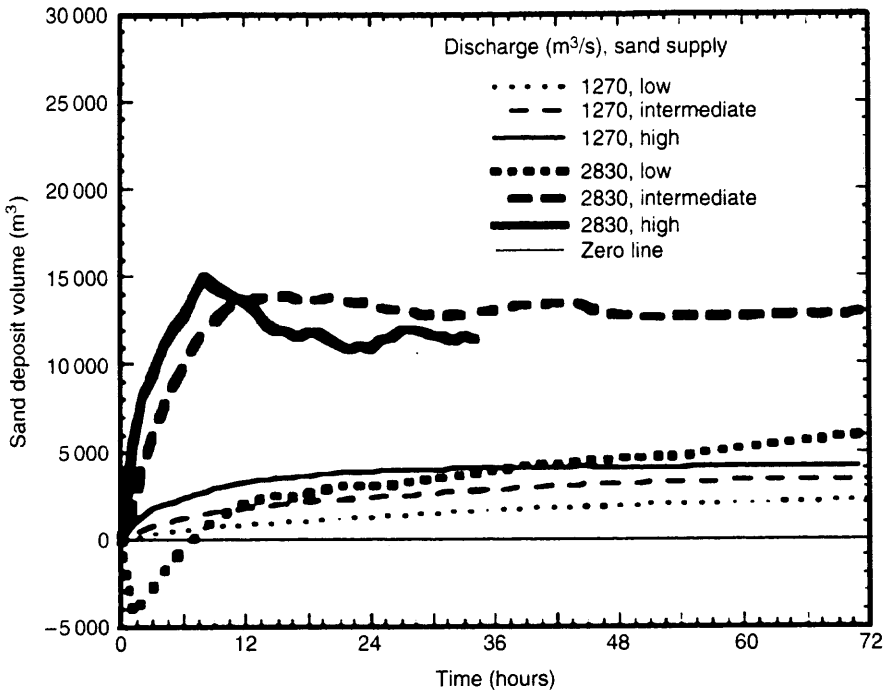

Figure 14.17 *Modelled change in sand deposit volume above the 708 m³/s stage in the Lower Tanner reach.*

14.6.4 Upper Unkar reach

14.6.4.1 Initial conditions

The Upper Unkar reach (Figures 14.18a and 14.19a) is about 1.6-km long down the channel centreline. A small recirculation zone is on river left near the reach inlet, and a deep hole in the main channel typically associated with recirculation zones in the upstream reaches is present here as well. The reach bends to the left and maintains a more consistent channel width at higher flow than the other study reaches. The most striking feature of this reach is the mid-channel bar that is inundated at higher flows, but forms an island at most typical dam releases (below about 500 m^3/s). This bar was formed by a debris flow that spilled gravels into the reach that have been reworked into the present configuration. At low flow, when the bar is an island, most of the discharge occupies the left channel.

A "No Visitation" label in river guides of Grand Canyon (e.g. Stevens, 1990) dramatically marks this reach as one of the most sensitive in Grand Canyon. The part of the reach labelled "J" on Figures 14.18 and 14.19 has been declared off limits to the public by the National Park Service because of the abundance of artefacts at that location. The gullies mapped by Hereford *et al.* (1991, 1993) also are located in this area (Figures 14.18 and 14.19).

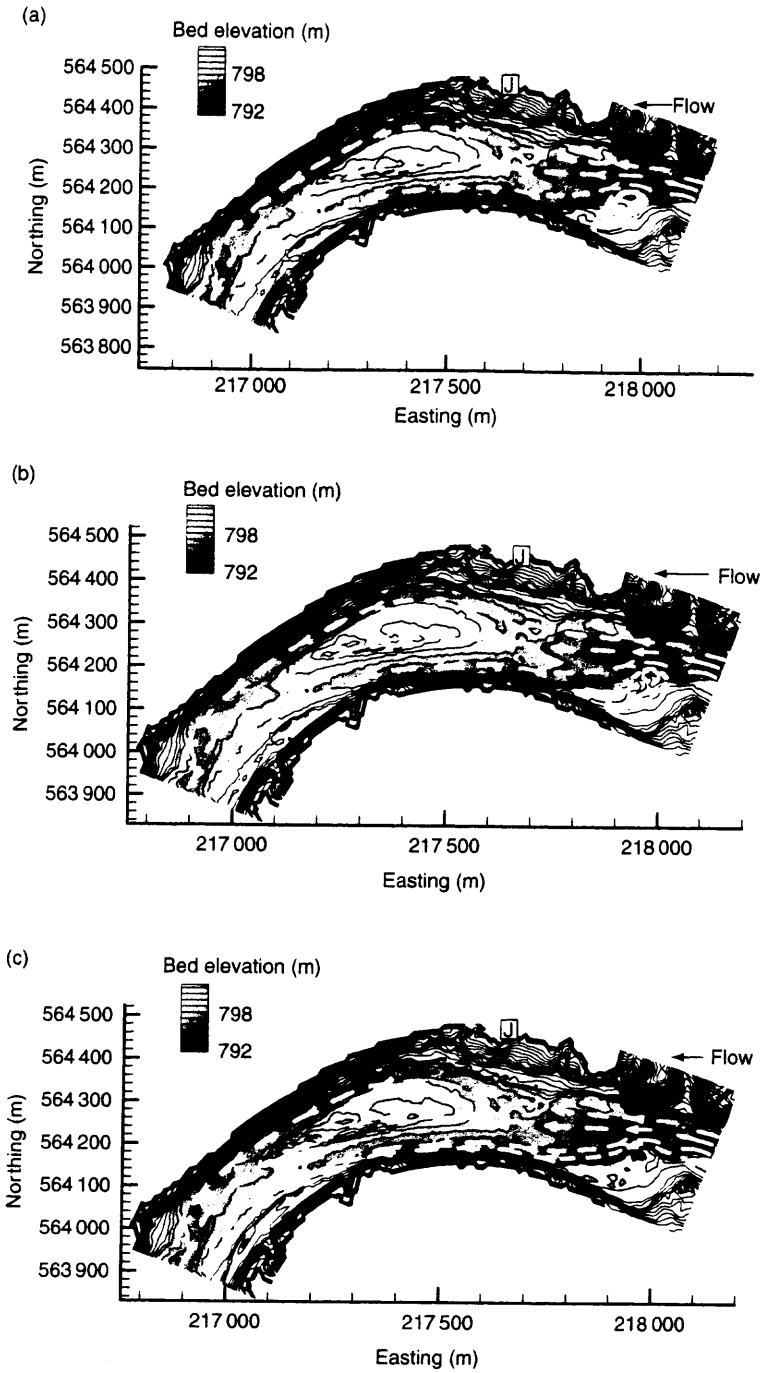

Figure 14.18 *Contour maps of the Upper Unkar reach at 1270 m³/s showing (a) the initial bed morphology (at time = 0), (b) the model prediction after 72 hours with the low (1983) sand supply and* $d_{50} = 0.24$ *mm, and (c) the model prediction after 72 hours with the high (1956) sand supply and* $d_{50} = 0.16$ *mm.*

14.6.4.2 Model predictions

The Upper Unkar reach contains a recirculation zone on river left near the reach inlet, but the area of interest with respect to gullies and vulnerable archaeological sites is on river right near the upper part of the mid-channel bar. The total sand deposition showed a clear separation between the deposition volume at 2830 m^3/s with the high sand supply and the other conditions (Figure 14.18, 14.19 and 14.20). At 2830 m^3/s with the high sand supply, substantial bars formed along the channel

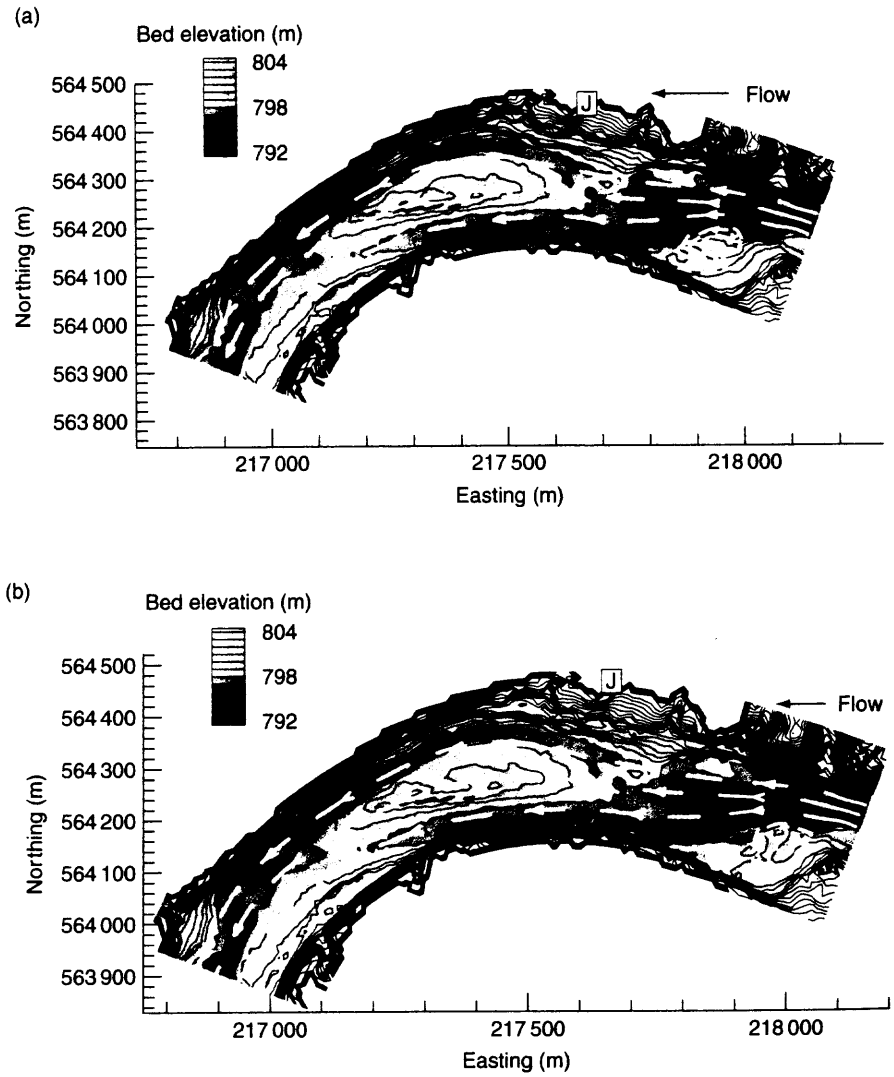

Figure 14.19 *Contour maps of the Upper Unkar reach at 2830 m^3/s showing (a) the initial bed morphology (at time = 0), (b) the model prediction after 72 hours with the low (1983) sand supply and d_{50} = 0.29 mm, and (c) the model prediction after 34 hours with the high (1956) sand supply and d_{50} = 0.14 mm.*

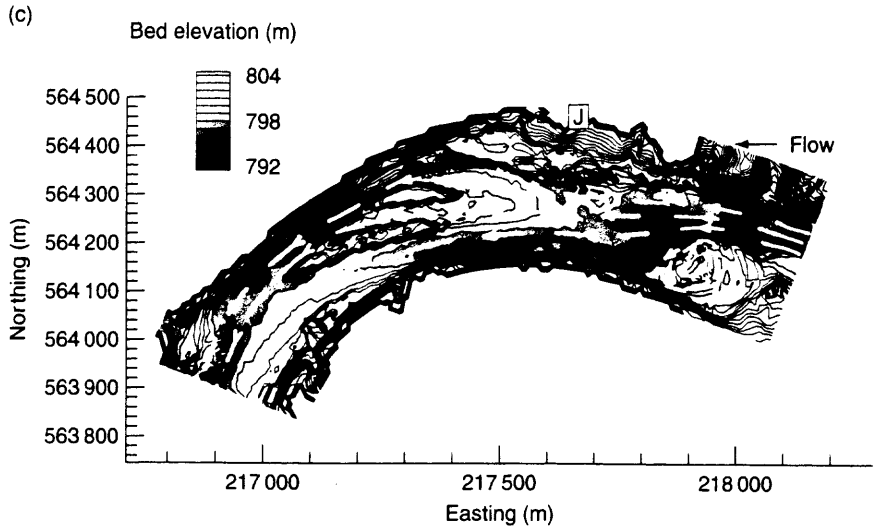

Figure 14.19 *(Continued).*

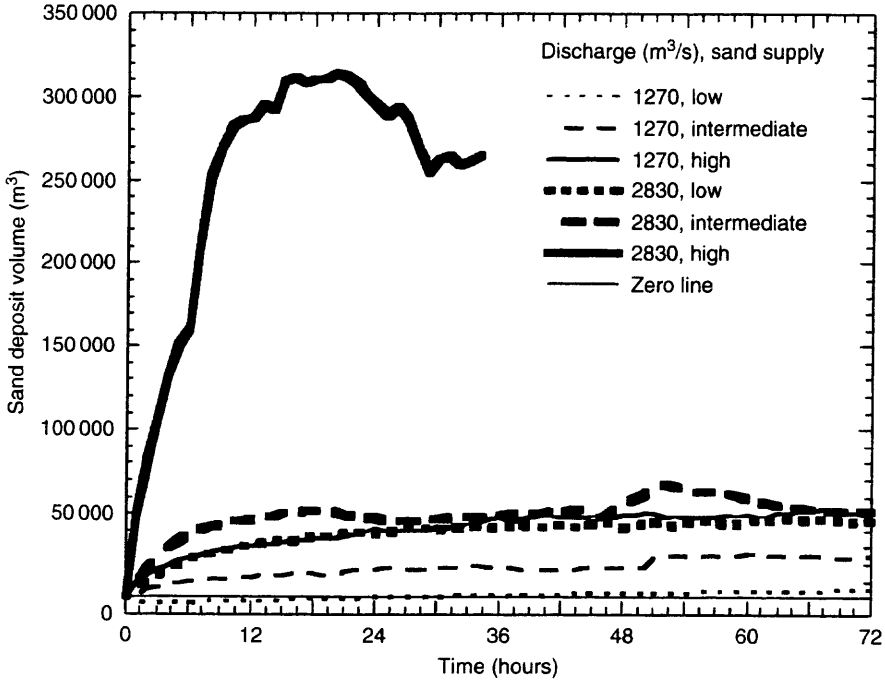

Figure 14.20 *Modelled change in sand volume as a function of time in the Upper Unkar reach.*

sides and around the tail end of the mid-channel gravel bar. At 2830 m^3/s with the low and intermediate sand supplies, the results were similar, with the deposit reaching capacity more rapidly with the intermediate sand supply. At 1270 m^3/s, the sand volume with the high sand supply matched the 2830 m^3/s results with the low and intermediate sand supplies. Total deposition at 1270 m^3/s with the low and intermediate sand supplies was relatively small.

Considering only the sand deposited above the 708 m^3/s stage, the differences between the volumes deposited with the three sand supplies at 1270 m^3/s were relatively small (Figure 14.21). At 1270 m^3/s, all three sand conditions converged to a similar sand volume; the deposit reached capacity within about 6–10 hours with the high and intermediate sand supplies, whereas the deposit steadily grew over most of the simulation with the low sand supply. The significance of accommodation space created by high stage was especially apparent in the results at 2830 m^3/s. At 2830 m^3/s, the sand deposits with the low and intermediate sand supplies were close to capacity after about 12 hours and reached a volume about seven times larger than with the lower discharge. With the high sand supply at 2830 m^3/s, sand deposit volume was nearly double the volume obtained with the two other sand conditions at 2830 m^3/s (Figure 14.21).

A more narrow focus on the deposits in region J, the critical region near the archaeological sites (Figure 14.22), showed a proportionately larger gap between the deposit volume at 2830 m^3/s with the high sand supply and the other cases than was evident for total depositional volumes for the entire reach (Figure 14.20). Total sand deposition near J for all cases except for the high sand supply at 2830 m^3/s and the low sand supply at 1270 m^3/s showed similar results at the end of the simulation.

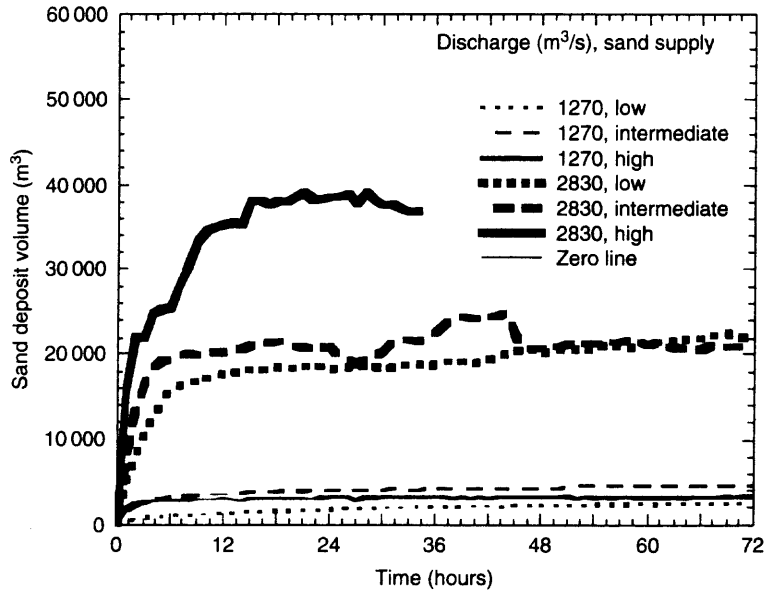

Figure 14.21 *Modelled change in sand deposit volume above the 708 m^3/s stage in the Upper Unkar reach.*

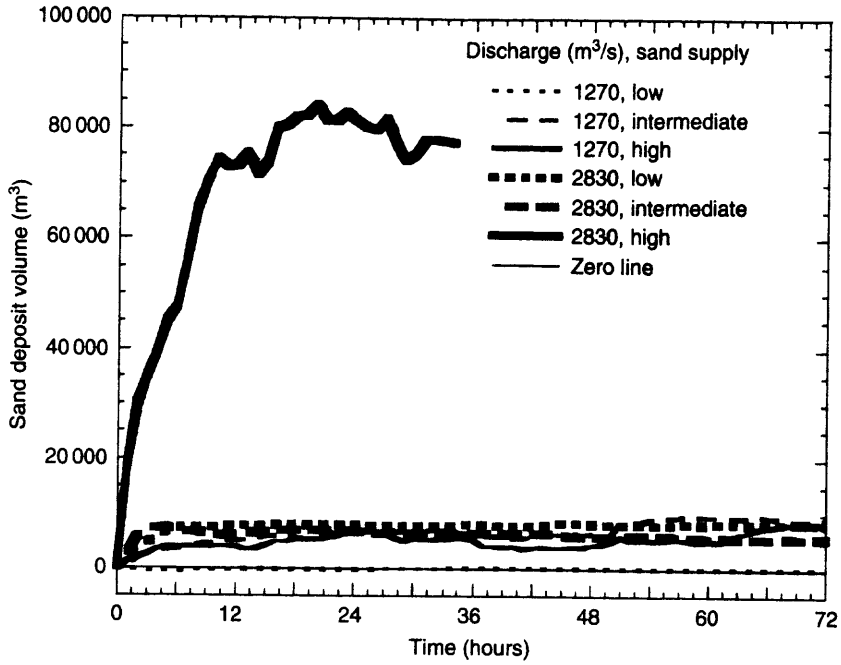

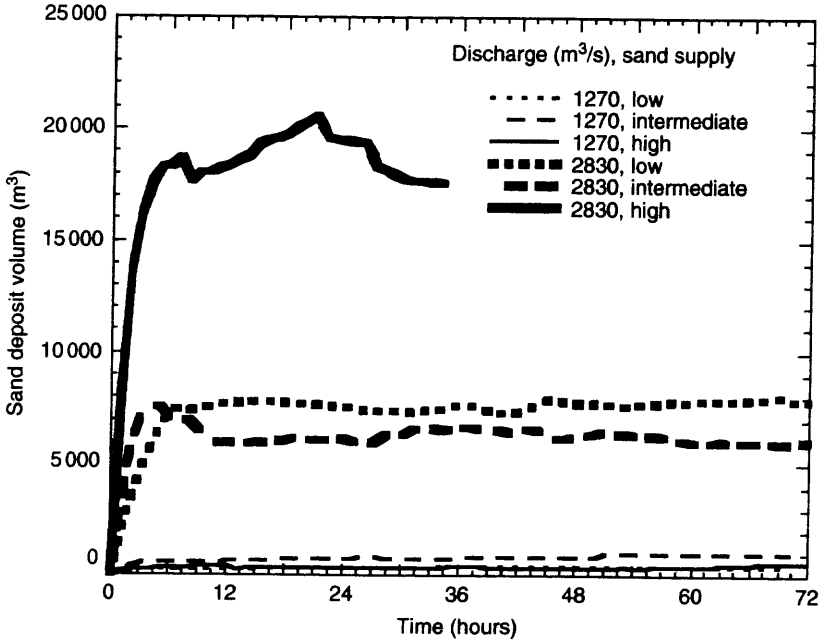

Figure 14.22 *Modelled changes in (a) total sand deposit volume and (b) the sand deposit volume above the 708 m³/s stage as functions of time at location J in the Upper Unkar reach.*

Sand deposits most likely to be of greatest benefit to artefact preservation were the deposits near J above the 708 m^3/s stage (Figure 14.22). Sand deposit volumes near J above 708 m^3/s were small at 1270 m^3/s for all sand supplies compared with the results at 2830 m^3/s. The increased accommodation space at 2830 m^3/s allowed for much larger deposits with the low and intermediate sand supplies than those formed at 1270 m^3/s. With the high sand supply, sand deposit volume near J above the 708 m^3/s stage was three times the sand deposit volume at 2830 m^3/s with the two other lower sand supplies. About half of the increase in total deposit volume for the reach shown in Figure 14.21 at 2830 m^3/s with the high sand supply was a result of increased deposition near J. In all cases, some deposition occurred in that region along the bank, aided in part by the presence of debris that was deposited upstream near the right bank during the same event that formed the mid-channel bar. With the highest sand supply, there was sufficient deposition to initiate substantial bars in the lee of that debris; thus large deposits were formed at the most advantageous site for the preservation of archaological artefacts.

14.7 Discussion

Modelling results show significant variability in deposition volumes relating to channel shape as well as to discharge and sand supply (Figure 14.23). In reaches

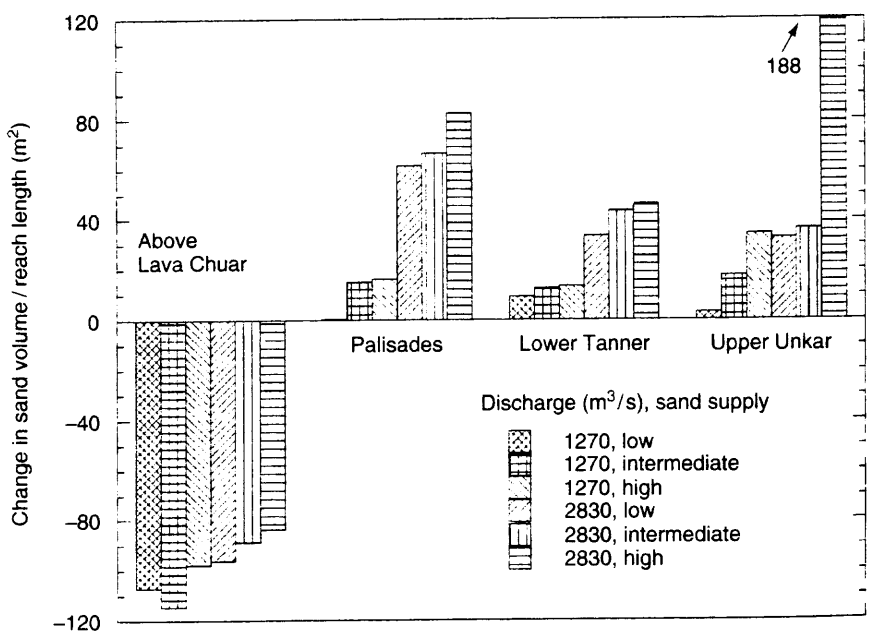

Figure 14.23 *Change in sand volume divided by reach length at the end of the modelling period. The change in sand volume is divided by reach length to facilitate the comparison of the effect of channel morphology on sand deposition and erosion.*

without significant recirculation zones, sand was stored in narrow bands along the channel sides under most conditions, primarily in the lee of channel irregularities. Sand volumes deposited above the 708 m^3/s stage in the Lower Tanner reach and in the critical right bank region (J) in the Upper Unkar reach were, at best, half the deposit volumes in the Above Lava Chuar and Palisades recirculation zones. Recirculation zones appear more consistent in response to increased discharge and variations in sand supply, and store more sediment for a given reach length. Trends in overall sand storage in reaches dominated by recirculation zones can be generalized, but in reaches where sand storage is dependent on finer-scale morphology of the channel sides, the trends are more variable.

High discharge releases. Higher flows, such as the 2830 m^3/s flow, tend to deposit sand in sheltered areas even with low sand supply. This is especially evident in the two upstream reaches in this study. Higher water discharges are significantly more effective in depositing sand in critical areas than lower discharges. This is a result of the greater sand transport rate for given sand conditions and, perhaps more significantly, the larger accommodation spaces created by higher stages.

High-flow duration. Deposition rate depends strongly on the volume of sand already present at a depositional site. Deposition rate falls rapidly as the site fills. As a result, high flows are most effective within the first day or two in filling depositional sites. Longer-duration high releases distribute sand more thoroughly within a depositional site, as pointed out by Anima *et al.* (1998), but are less efficient at utilizing sand in transport.

Sand supply. High sand concentrations, such as would occur during significant tributary flow, would be most effective in forming significant deposits in critical areas. The possibility and potential advantages of dam releases timed to coincide or shortly follow tributary flows were considered by the authors of the EIS (US Department of Interior, 1995), and were reiterated by Lucchitta and Leopold (1999) with particular emphasis on flows in the Little Colorado River. Careful analyses of sand deposits, sand transport processes and suspended sand measurements (Rubin *et al.*, 1998; Topping *et al.*, 2000a,b) have provided a process-based explanation of the importance of tributary inputs to replenishing sand resources, especially those in Marble Canyon that rely primarily on the sand inputs from the Paria River, and a quantification of the potential benefits of high releases associated with tributary inputs. Releasing high flows during or shortly following significant tributary flows would also increase the supply of fine-grained sediment, which would increase the stability of the deposits (as pointed out by Richard Hereford, USGS, oral communication, 1998). High discharges increase the total volume of the deposit and place the sand higher up the channel bank and, therefore, would place a larger volume within the gully mouths.

It is important to note that these study sites are in a relatively sand-rich reach compared with the channel above the confluence with the Little Colorado River. High discharges may deposit sand at many sites in this region, even with a low sand supply; but upstream of the confluence with the Little Colorado River, the lower sand supply in the absence of significant flow in the Paria River would make that reach more vulnerable to erosion (Schmidt, 1999; Topping *et al.*, 2000a,b).

Influence of channel shape on deposition volume. Results in region A in the Above Lava Chuar reach are consistent with the conceptual model of Melis (1997) for the relation between shoreline types and fan–eddy attributes and the potential for sand storage. Melis (1997) suggested that the greatest potential for sand storage would occur in reaches with the greatest density of debris fans and downstream from the tightest channel constrictions, and that the least potential for sand storage would occur in reaches with steep shorelines and few debris fans. The model results for these four reaches support the conclusion that recirculation zones are the most effective sites for storing large volumes of sand that are likely to endure on a time scale of months to years. The parts of these deposits that are beneath the water surface during normal dam operation, however, are still subject to erosion at lower discharges by scour, although at a much slower rate than occurs in the main channel. These inundated deposits may also erode rapidly during routine dam operation (Cluer, 1995). Deposits along the channel sides that are perched above the 708 m^3/s stage, albeit smaller than the recirculation deposits, may have greater potential for preservation. Little is currently known about the rates at which erosive processes, such as aeolian transport, operate.

Potential negative impacts of high flows. The cases studied so far have led to the generalizations listed above. Particular sites may respond differently. Schmidt *et al.* (1999) and Hazel *et al.* (1997, 1999) documented considerable variation in response to the 1996 test flow within reaches with similar morphology. Even at a given site, periodic mass failure of rapidly accumulated sand deposits can lead to a temporal variability in sand deposit volume (Andrews *et al.*, 1999). Widening of the main channel flow at higher stages may diminish deposits formed at lower discharges in some reaches, as shown in A in the Above Lava Chuar reach and as was suggested by Melis (1997). This is especially likely if high releases are necessary to lower Lake Powell, as happened during 1983–1984 when sustained high flows peaking at 2720 m^3/s caused erosion at some archaeological sites (US Department of Interior, 1995). Although results so far have shown deposition under most conditions in sheltered areas, such as recirculation zones, under some conditions erosion can occur within recirculation zones (Joseph Hazel, Northern Arizona University, oral communication, 1999). Erosion in recirculation zones is most likely to occur with deeper flows, caused by some combination of increased stage and initial low elevation of the sand deposit, if the channel morphology is conducive to high flow velocities and is combined with low sand supply in the main stem. Erosion and deposition in reaches with gradually varying channel width are more likely to show greater sensitivity to variations in water and sand discharge.

14.8 Conclusion

The model used in this study provides a physically based, predictive method for examining the effects of dam releases and sand supplies on sand deposits. Predictions of changes in sand bars can be made at specific sites and general trends can be inferred from modelling results over a range of conditions and at multiple sites. The model was constructed with sufficient complexity to represent processes with an accuracy commensurate with the purpose of the study using available computational power.

Acknowledgements

The authors thank Ruth Lambert, Cultural Resources Program Manager at the GCMRC, for funding and for her support of this project. Billy Elwanger, Mark Gonzalez, Steve Lamphear, Mimi Murov, Nels Niemi, Barbara Ralston and Don Scarbrough made indispensable contributions to the field work. Ted Melis, David Topping, Kate Thompson and Andre Potochnik contributed with helpful scientific discussions and insights. Reviews by Ned Andrews, Paul Bates, Rob Ferguson, Julie Graf, Steve Longsworth, Ted Melis, Melissa Ray and Tracey Suzuki improved the manuscript.

References

Andrews, E.D., C.E. Johnston, J.C. Schmidt and M. Gonzales, 1999, Topographic evolution of sand bars, in Webb, R.H., Schmidt, J.C., Marzolf, G.R. and Valdez, R.A. (eds), *The Controlled Flood in Grand Canyon: Washington, D.C.*, American Geophysical Union, Geophysical Monograph 110, pp. 117–130.

Anima, R.J., M.S. Marlow, D.M. Rubin and D.J. Hogg, 1998, Comparison of Sand Distribution between April 1994 and June 1996 along Six Reaches of the Colorado River in Grand Canyon, Arizona, *U.S. Geological Survey Open-File Report 98-141*, 33pp.

Bennett, J.P., 1995, Algorithm for resistance to flow and transport in sand-bed channels, *Journal of Hydraulic Engineering*, ASCE, 121(8), pp. 578–590.

Beus, S.S., S.W. Carothers and C.C. Avery, 1985, Topographic changes in fluvial terrace deposits used as campsite beaches along the Colorado River in Grand Canyon, *Journal of the Arizona–Nevada Academy of Science*, 20, pp. 111–120.

Cluer, B.L., 1995, Cyclic fluvial processes and bias in environmental monitoring, Colorado River in Grand Canyon, *Journal of Geology*, 95(103), pp. 411–421.

Dietrich, W.E., 1982, Flow, boundary shear stress, and sediment transport in a river meander, Unpublished PhD dissertation, University of Washington, Seattle, Washington.

Dolan, R., A.D. Howard and D. Trimble, 1978, Structural control of rapids and pools of the Colorado River in the Grand Canyon, *Science*, 202, pp. 629–631.

Environmental Systems Research Institute, Inc., 1991, ARC/INFO User's Guide – Surface Modeling with TIN^{TM}, Environ. Syst. Res. Inst., Inc., Redlands, Calif.

Hazel, J.E., M. Kaplinski, M.F. Manone, R.A. Parnell, A.R. Dale, J. Ellsworth and L. Dexter, 1997, The effects of the 1996 Glen Canyon Dam beach/habitat-building test flow on Colorado River sand bars in Grand Canyon, *Final Report to Glen Canyon Environmental Studies.*

Hazel, J.E., M. Kaplinski, R.A. Parnell, M.F. Manone and A.R. Dale, 1999, Topographic and bathymetric changes at thirty-three long-term study sites, in Webb, R.H., Schmidt, J.C., Marzolf, G.R. and Valdez, R.A. (eds), *The Controlled Flood in Grand Canyon: Washington, D.C.*, American Geophysical Union, Geophysical Monograph, 110, pp. 161–183.

Hereford, R., 1996, Map showing surficial geology and geomorphology of the Palisades Creek area, Grand Canyon, National Park, Arizona, Miscellaneous Investigations Series, Map I-2449, *U.S. Geological Survey*, 1 sheet, scale 1:2000.

Hereford, R., H.C. Fairley, K.S. Thompson and J.R. Balsom, 1991, The effect of regulated flows on erosion of archeologic sites at four areas on eastern Grand Canyon National Park, Arizona: A preliminary analysis, *U.S. Geological Survey Administrative Report*, 36pp.

Hereford, R., H.C. Fairley, K.S. Thompson, J.R. Balsom, 1993, Surficial geology, geomorphology, and erosion of archaeological sites along the Colorado River, eastern Grand

Canyon, Grand Canyon National Park, Arizona, *U.S. Geological Survey Open-File Report 93-517*. 46pp. 2 sheets.

Hereford, R., K.S. Thompson, K.J. Burke and H.C. Fairley, 1996, Tributary debris fans and the late Holocene alluvial chronology of the Colorado River, eastern Grand Canyon, Arizona, *Geological Society of America Bulletin*, 108(1), 3–19.

Hereford, R., K.J. Burke and K.S. Thompson, 1998, Quaternary geology and geomorphology of the Nankoweap Rapids area, marble Canyon, Arizona, Geologic Investigations Series, Map I-2608, *U.S. Geological Survey*, 18pp. 1 sheet, scale 1:2000.

Howard, A.D. and R. Dolan, 1981, Geomorphology of the Colorado River in the Grand Canyon, *Journal of Geology*, 89(3), pp. 269–298.

Kearsley, L.H., R.D. Quartaroli and M.C. Kearsley, 1999, Changes in the number and size of campsites as determined by inventories and measurement, in Webb, R.H., Schmidt, J.C., Marzolf, G.R. and Valdez, R.A. (eds), *The Controlled Flood in Grand Canyon: Washington, D.C.*, American Geophysical Union, Geophysical Monograph 110, pp. 147–159.

Keulegan, G.H., 1938, Laws of turbulent flows in open channels, Res. Paper RP1151, National Bureau of Standards, 21, pp. 707–741.

Korman, J., S.M. Wiele and M. Torizzo, 2004, Modeling the Effect of Discharge on Habitat Quality and Dispersal of Juvenile Humpback Chub (*Gila cypha*) in the Colorado River in Grand Canyon, Regulated Rivers, 20, pp. 379–400.

Lucchitta, I. and L.B. Leopold, 1999, Floods and sandbars in the Grand Canyon, *GSA Today*, 9(4), pp. 1–7.

McLean, S.R., 1992, On the calculation of suspended sediment load for noncohesive sediments, *Journal of Geophysical Research*, 97(C4), pp. 5759–5770.

Melis, T.S., 1997, Geomorphology of debris flows and alluvial fans in Grand Canyon National Park and their influence on the Colorado River below Glen Canyon Dam, Arizona, PhD dissertation, University of Arizona, Tucson, 490pp.

Melis, T.S., R.H. Webb, P.G. Griffiths and T.J. Wise, 1994, Magnitude and frequency data for historic debris flows in Grand Canyon National Park and vicinity, Arizona, *U.S. Geological Survey Water Resources Investigation Report 94-4214*, 285pp.

Meyer-Peter, E. and R. Müller, 1948, *Formulas for Bed-Load Transport*, International Association for Hydraulic Research, Second Meeting, Stockholm.

Nelson, J.M. and J.D. Smith, 1989a, Evolution and stability of erodible channel beds, in Ikeda, S. and Parker, G. (eds), *River Meandering*, pp. 321–377.

Nelson, J.M. and J.D. Smith, 1989b, Mechanics of flow over ripples and dunes, *Journal of Geophysical Research*, 89(C6), pp. 8146–8162.

Patankar, S.V., 1980, *Numerical Heat Transfer and Fluid Flow*, Hemisphere, Washington, DC, 197pp.

Powell, J.W., 1897, *The Exploration of the Colorado River and Its Canyons*, Penguin Books, New York, 291pp.

Rouse, H., 1937, Modern conceptions of the mechanics of turbulence, *Transactions of the American Society of Civil Engineers*, 102, pp. 463–543.

Rubin, D.M., J.M. Nelson and D.J. Topping, 1998, Relation of inversely graded deposits to suspended-sediment grain-size evolution during the 1996 flood experiment in Grand Canyon, *Geology*, 26(2), pp. 99–102.

Rubin, D.M., D.J. Topping, J.C. Schmidt, T. Melis, J. Hazel and M. Kaplinski, 2002, Results of the 1996 experimental flow in Grand Canyon, EOS.

Schmidt, J.C., 1987, Geomorphology of alluvial-sand deposits, Colorado River, Grand Canyon National Park, Arizona, Unpublished PhD dissertation, Johns Hopkins University, Baltimore, Maryland.

Schmidt, J.C., 1999, Summary and synthesis of geomorphic studies conducted during the 1996 controlled flood in Grand Canyon, in Webb, R.H., Schmidt, J.C., Marzolf, G.R. and

Valdez, R.A. (eds), *The Controlled Flood in Grand Canyon: Washington, D.C.*, American Geophysical Union, Geophysical Monograph 110, pp. 329–341.

Schmidt, J.C. and J.B. Graf, 1990, Aggradation and degradation of alluvial sand deposits, 1965 to 1986, Colorado River, Grand Canyon National Park, Arizona, *U.S. Geological Survey Professional Paper 1493*, 74pp.

Schmidt, J.C. and D.M. Rubin, 1995, Regulated streamflow, fine-grained deposits, and effective discharge in canyon with abundant debris fans, in J.E. Costa *et al.* (eds), *Natural and Anthropogenic Influences in Fluvial Geomorphology: The Wolman Volume*, Geophysical Monograph Series, American Geophysical Union, Washington, DC, 89, pp. 177–195.

Schmidt, J.C. and M.F. Leschin, 1995, Geomorphology of post-Glen Canyon Dam fine-grained alluvial deposits of the Colorado River in the Point Hansbrough and Little Colorado River confluence study reaches in Grand Canyon National Park, Arizona, *Report to Glen Canyon Environmental Studies.*

Schmidt, J.C., P.E. Grams and M.F. Leschin, 1999, Variation in the magnitude and style of deposition and erosion in three long (8–12 km) reaches as determined by photographic analysis, in Webb, R.H., Schmidt, J.C., Marzolf, G.R. and Valdez, R.A. (eds), *The Controlled Flood in Grand Canyon: Washington, D.C.*, American Geophysical Union, Geophysical Monograph 110, pp. 185–283.

Shields, A., 1936, Application of similarity principles and turbulence research to bed-load movement (in German), Mitteil. Preuss. Versuchanst. Wasser, Erd, Schiffsbau, Berlin, 26.

Smith, J.D. and S.R. McLean, 1977, Spatially averaged flow over a wavy surface, *Journal of Geophysical Research*, 82(12), pp. 1735–1746.

Smith, J.D. and S.R. McLean, 1984, A model for flow in meandering streams, *Water Resources Research*, 20(9), pp. 1301–1315.

Stevens, L.E., 1990, *The Colorado River in Grand Canyon, A Guide*, Red Lake Books, Flagstaff, Arizona, 115pp.

Thompson, K. and A. Potochnik, 1997, Proposal to test and apply a geomorphic model related to erosion of pre-dam river terraces in the Colorado River ecosystem containing cultural materials, proposal to the Cultural Resources Program, Grand Canyon Monitoring and Research Center.

Thompson, K. and A. Potochnik, 2000, Development of a geomorphic model to predict erosion of pre-dam Colorado River terraces containing archaeological resources, prepared for Grand Canyon Monitoring and Research Center, Flagstaff, Arizona.

Thompson, K., K. Burke and A. Potochnik, 1997, Effects of the beach-habitat building flow and subsequent interim flows from Glen Canyon Dam on Grand Canyon camping beaches, 1996: A repeat photography study by Grand Canyon river guides (adopt-a-beach program), *Administrative Report to the Grand Canyon Monitoring and Research Center*, Flagstaff, Arizona.

Topping, D.J., 1997, Flow, sediment transport, and channel geomorphic adjustment in the Grand Canyon, Arizona gage reach of the Colorado River during the Grand Canyon flood experiment: Abstracts and executive summaries, Symposium on the 1996 Glen Canyon Dam Beach/Habitat-Building Flow, Flagstaff, Arizona.

Topping, D.J., D.M. Rubin and L.E. Vierra Jr, 2000a, Colorado river sediment transport, 1, Natural sediment supply limitation and the influence of Glen Canyon Dam, *Water Resources Research*, 36(2), pp. 515–542.

Topping, D.J., D.M. Rubin, J.M. Nelson, P.J. Kinzel III and I.C. Corson, 2000b, Colorado river sediment transport, 2, Systematic bed-elevation and grain-size effects of sand supply limitation, *Water Resources Research*, 36(2), pp. 543–570.

US Department of Interior, 1995, Operation of Glen Canyon Dam: Final Environmental Impact Statement, *Colorado River Storage Project*, Coconino County, Arizona, 337pp. and appendices, Salt Lake City, Utah.

van Rijn, L.C., 1984, Sediment transport. Part III: suspended load transport, *Journal of Hydrological Engineering*, ASCE, 110(11), pp. 1613–1641.

Webb, R.H., P.T. Pringle and G.R. Rink, 1989, Debris flows from tributaries of the Colorado River, Grand Canyon National Park, Arizona, *U.S. Geological Professional Paper 1492*, 39pp.

Webb, R.H., D.L. Wegner, E.D. Andrews, R.A. Valdez and D.T. Patten, 1999, Downstream effects of Glen Canyon Dam on the Colorado River in Grand Canyon: A review, in Webb, R.H., Schmidt, J.C., Marzolf, G.R. and Valdez, R.A. (eds), *The Controlled Flood in Grand Canyon: Washington, D.C.*, American Geophysical Union, Geophysical Monograph 110, pp. 131–145.

Wiberg, P.L. and D.M. Rubin, 1985, Bed roughness produced by saltating sediment, *Journal of Geophysical Research*, 94(C4), pp. 5011–5016.

Wiele, S.M., 1997, Modeling of flood-deposited sand distributions for a reach of the Colorado River below the Little Colorado River, Grand Canyon, Arizona, *U.S. Geological Survey Water-Resources Investigation Report 97-4168*, 15pp.

Wiele, S.M. and J.D. Smith, 1996, A reach-averaged model of diurnal discharge wave propagation down the Colorado River through the Grand Canyon, *Water Resources Research*, 32(5), pp. 1375–1386.

Wiele, S.M., J.B. Graf and J.D. Smith, 1996, Sand deposition in the Colorado River in the Grand Canyon from flooding of the Little Colorado River, *Water Resources Research*, 32(12), pp. 3579–3596.

Wiele, S.M., E.D. Andrews and E.R. Griffin, 1999, The effect of sand concentration on depositional rate, magnitude, and location, in Webb, R.H., Schmidt, J.C., Marzolf, G.R. and Valdez, R.A. (eds), *The Controlled Flood in Grand Canyon: Washington, D.C.*, American Geophysical Union, Geophysical Monograph 110, pp. 131–145.

Wilson, R.T., 1986, *Sonar patterns of Colorado River bed, Grand Canyon*, Proceedings of the Fourth Federal Interagency Sedimentation Conference, Las Vegas, Nevada, 2, pp. 5-133–5-142.

Yeatts, M., 1996, High elevation sand deposition and retention from the 1996 spike flow: An assessment for cultural resources stabilization, *Final Report to Glen Canyon Environmental Studies*.

Yeatts, M., 1998, 1997, Data recovery at five sites in the Grand Canyon, *Final Report to the Bureau of Reclamation*, Salt Lake City, Utah and Grand Canyon Monitoring and Research Center, Flagstaff, Arizona.